

Supramolecular Materials from Triblock Rodcoil Molecules Containing Phenylene Vinylene

Gregory N. Tew, Martin U. Pralle, and Samuel I. Stupp*

Contribution from the Departments of Materials Science and Engineering and Chemistry, Northwestern University, Evanston, Illinois 60208

Received May 6, 1999

Abstract: We report here on the synthesis and characterization of several triblock rodcoil molecules containing conformationally rigid and flexible sequences and luminescent chromophores based on phenylene vinylene. The molecules consist of blocks of oligostyrene, oligoisoprene, and a rigid rod block. The synthesis of the rod blocks required the preparation of new phenylene vinylene oligomers. On the basis of electron microscopy and X-ray diffraction experiments, these systems were found to self-organize into supramolecular nanostructures which in turn assemble into monolayers. The nanostructures have diameters between 3.5 and 5 nm, and the regularity of the nanostructures depends on rod-to-coil volume fraction. The layer spacing of one system is 6.0 nm when cast from solution but increases to 7.8 nm upon annealing at 150 °C, possibly as a result of an increase in aggregation number. Interestingly, the formation of supramolecular nanostructures and the observed hierarchical order in the materials formed by rodcoil molecules can be completely suppressed by lowering the rod-to-coil volume ratio. When the chemical structure of rod segments is changed, the nanostructures formed can undergo a drastic increase in aspect ratio. These changes in shape maybe linked to different tendencies for aggregation among rod segments. Absorption and emission spectra of supramolecular solids are similar to dilute solution spectra and different from those of similar disordered materials.

Introduction

Supramolecular chemistry is emerging as a powerful tool for the creation of regular organic nanostructures. Previous work has reported on self-assembly of well-defined structures in the range of 1–10 kilodaltons (kDa) and a few nanometers in dimensions.^{1,2} However, the formation of regular structures with dimensions in the range of 1–100 nanometers and molecular weights of 10¹–10⁴ kDa remains a challenge. Our laboratory recently reported the self-organization of nanostructures in this molar mass range which have narrow size distributions.³ The field of supramolecular chemistry commonly utilizes different strategies to assemble structures beyond the molecule that include ionic and hydrogen bonds,^{4–8} metal coordination chemistry,^{9,10} and nonspecific interactions such as van der Waals and π – π stacking.^{3,11}

* To whom correspondence should be addressed. This work was carried out at the University of Illinois at Urbana-Champaign.

(1) Lehn, J. M. *Supramolecular Chemistry*; VCH Press: New York, 1995.

(2) Whitesides, G. M.; Mathias, J. P.; Seto, C. T. *Science* **1991**, *254*, 1312–1319.

(3) Stupp, S. I.; LeBonheur, V.; Walker, K.; Li, L. S.; Huggins, K.; Keser, M.; Amstutz, A. *Science* **1997**, *276*, 384–389.

(4) Sijbesma, R. P.; Beijer, F. H.; Brunsveld, L.; Folmer, B. J. B.; Hirschberg, J. H. K. K.; Lange, R. F.; Lowe, J. K. L.; Meijer, E. W. *Science* **1997**, *278*, 1601–1604.

(5) Zimmerman, S. C.; Zeng, F.; Reichert, D. E. C.; Kolotuchin, S. V. *Science* **1996**, *271*, 1095–1098.

(6) Whitesides, G. M.; Simanek, E. E.; Mathias, J. P.; Seto, C. T.; Chin, D. N.; Mammen, M.; Gordon, D. M. *Acc. Chem. Res.* **1995**, *28*, 37–44.

(7) Kato, T.; Frechet, J. M. J. *J. Am. Chem. Soc.* **1989**, *111*, 8533–8534.

(8) Kumar, U.; Kato, T.; Frechet, J. M. J. *J. Am. Chem. Soc.* **1992**, *114*, 6630–6639.

(9) Olenyuk, B.; Whiteford, J. A.; Stang, P. J. *J. Am. Chem. Soc.* **1996**, *118*, 8221–8230.

(10) Funeriu, D. P.; Lehn, J. M.; Baum, G.; Fenske, D. *Chem. Eur. J.* **1997**, *3*, 99–104.

Our group focuses on design and synthesis of molecules that organize into supramolecular objects as the building blocks of materials.^{3,12–14} In one approach to such supramolecular materials we utilized the self-organization of diblock polymers into various morphologies that include discrete nanostructures.^{15,16} One of these copolymers is composed of oligoisoprene segments covalently connected to a rigid rod compound and termed rodcoil polymers since one block is conformationally flexible and the other has stiff, rodlike character. Most recently, we extended the self-organization of these diblock copolymers to triblock rodcoil molecules where two of the blocks are now conformationally flexible and the third block is a rigid, crystallizable segment.^{3,14,17}

The formation of nanostructures from these triblock systems may be quite complex, encompassing a variety of factors. These may include entropic effects associated with coil segments, rod crystallization, and sterically induced repulsive forces among coil segments. The diblock coil contains extensive chemical diversity in sharp contrast to the rod segment which is a chemical compound. The tendency for π – π stacking among rod segments drives the system to aggregate and crystallize. Aggregation of the rod blocks must exclude the chemically

(11) Philip, D.; Stoddart, J. F. *Angew. Chem., Int. Ed. Engl.* **1996**, *35*, 1154–1196.

(12) Stupp, S. I.; Son, S.; Li, L. S.; Lin, H. C.; Keser, M. *J. Am. Chem. Soc.* **1995**, *117*, 5212–5227.

(13) Zubarev, E. R.; Pralle, M. U.; Li, L. M.; Stupp, S. I. *Science* **1999**, *283*, 523–526.

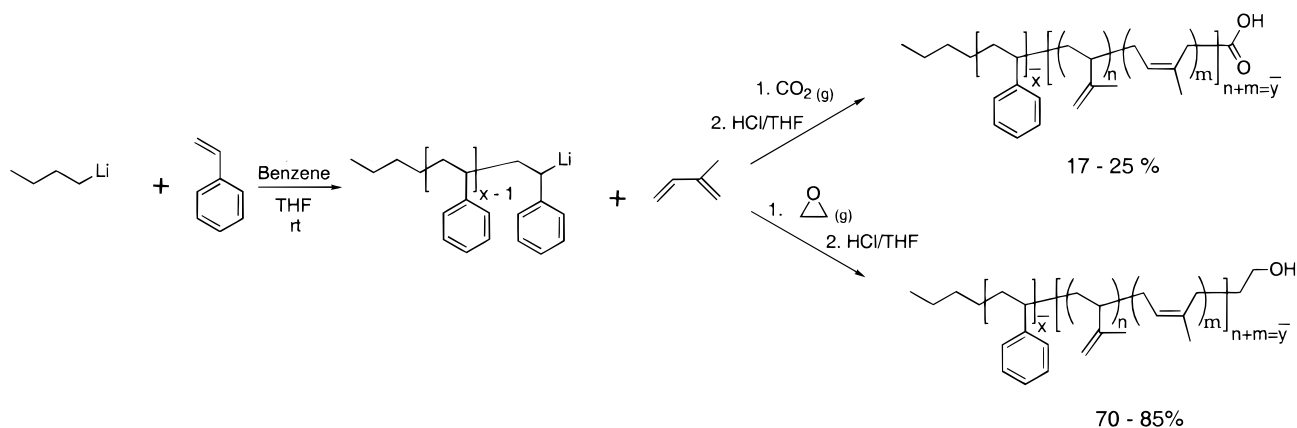
(14) Tew, G. N.; Pralle, M. U.; Stupp, S. I. *Angew. Chem., Int. Ed.* **1999**, in press.

(15) Radzilowski, L. H.; Stupp, S. I. *Macromolecules* **1994**, *27*, 7747–7753.

(16) Radzilowski, L. H.; Carragher, B. O.; Stupp, S. I. *Macromolecules* **1997**, *30*, 2210–2119.

(17) Tew, G. N.; Li, L. M.; Stupp, S. I. *J. Am. Chem. Soc.* **1998**, *120*, 5601–5602.

Scheme 1



diverse coils from their crystalline domain. As crystallization of rod blocks occurs, the entropy of coil blocks may be increasingly compromised as a result of stronger steric repulsion. We believe this effect limits aggregate size and is greatly enhanced in coil segments with large cross-sectional area relative to that of rod segments. Our strategy in creating supramolecular objects employs nonspecific interactions such as van der Waals, π - π aromatic stacking, and entropic effects to guide self-organization, a marked departure from the majority of previous self-assembly work. One of the important goals in materials chemistry is the creation of regularly shaped novel objects such as molecular tubes, large diameter rods, and two-dimensional (2-D) supramolecular sheets. These objects are likely to self-order into large arrays due to their regular shape and exhibit new properties as a result of both their discrete dimensions and three-dimensional (3-D) organization.

As a result of great interest in the electronic and optical properties of poly(*p*-phenylene vinylene) (PPV), a variety of structural modifications to this polymer have been reported.¹⁸ Some approaches to PPV derivatives include the addition of flexible or bulky side chains, generally at the 2 and 5 positions, to increase solubility and processability. There have been also structural changes reported along the conjugated backbone to modulate electronic and optical properties of the material, as well as the synthesis of block copolymers.¹⁹⁻²² In addition to PPV derivatives, there is a small collection of reports on oligomeric phenylene vinylene (PV)²³⁻³¹ derivatives as well as

poly(phenylene vinylene) dendrimers.^{32,33} However, little work has been reported on unsubstituted oligomers of phenylene vinylene mainly because of the extreme insolubility of these materials.³⁴ Phenylene vinylene is a robust material and a strong fluorophore and thus an ideal system for the creation of novel electronic and photonic materials. Moreover, PV is an excellent candidate as a rod block within our triblock architecture because its all-*trans* architecture leads to a rigid, linear, and conjugated molecular backbone. We report here on the synthesis and self-organization of a variety of novel triblock molecules containing oligostyrene, oligoisoprene, and unsubstituted oligomers of phenylene vinylene.

Results and Discussion

Synthesis. Several triblock rodcoil molecules have been synthesized containing different compositions of a diblock styrene-*b*-isoprene coil and various photonically active rod blocks. These molecules were designed to study the chemical and architectural features that lead to nanostructured supramolecular materials using the triblock architecture, and also to explore nanostructured materials with interesting electronic and optical properties. Scheme 1 shows the synthesis of the oligo styrene-*b*-isoprene coil segment by living anionic polymerization which allows control over the average chain length and molecular composition of the backbone through the molar ratios of initiator and monomer used in the reaction.³⁵ A variety of diblock coil lengths and compositions were synthesized as reported in Table 1. These diblock coils were synthesized under standard conditions where the polarity of the solvent was controlled to provide reasonable reaction rates for the polymerization and predictable isoprene addition products.³⁶ The diblock coil should have a distribution of molar masses near or slightly narrower than a Poisson type distribution under these reaction conditions.³⁷ When the polydispersity index (PDI) was measured for the diblock material, the PDI ranged between 1.04 and 1.12 based on gel permeation chromatography (GPC) using polystyrene standards. While GPC indicates a narrow molecular

(18) Kraft, A.; Grimsdale, A. C.; Holmes, A. B. *Angew. Chem., Int. Ed.* **1998**, *37*, 402-428.

(19) Harrison, N. T.; Baigent, D. R.; Samuel, I. D. W.; Friend, R. H.; Grimsdale, A. C.; Moratti, S. C.; Holmes, A. B. *Phys. Rev. B* **1996**, *53*, 15815-15821.

(20) Hide, F.; Schwartz, B. J.; Díaz-García, M. A.; Heeger, A. J. *Synth. Met.* **1997**, *91*, 35-40.

(21) Yang, Z.; Karasz, F. E.; Geise, H. J. *Macromolecules* **1993**, *26*, 6, 6570-6575.

(22) Yang, Z.; Sokolik, I.; Karasz, F. E. *Macromolecules* **1993**, *26*, 1188-1190.

(23) Maddux, T.; Li, W.; Yu, L. *J. Am. Chem. Soc.* **1997**, *119*, 844-845.

(24) Li, W.; Wang, H.; Yu, L.; Morkved, T. L.; Jaeger, H. M. *Macromolecules* **1999**, *32*, 3034-3044.

(25) Klärner, G.; Former, C.; Yan, X.; Richert, R.; Müllen, K. *Adv. Mater.* **1996**, *8*, 932-935.

(26) Gill, R. E.; Meetsma, A.; Hadziioannou, G. *Adv. Mater.* **1996**, *8*, 212-214.

(27) Gebhardt, V.; Bacher, A.; Thelakkat, M.; Stalmach, U.; Meier, H.; Schmidt, H.-W.; Haarer, D. *Synth. Met.* **1997**, *90*, 123-126.

(28) Oldham, W. J. J.; Miao, Y. J.; Lachicotte, R. L.; Bazan, G. C. *J. Am. Chem. Soc.* **1998**, *120*, 419-420.

(29) Campbell, T. W.; McDonald, R. N. *J. Org. Chem.* **1959**, *24*, 1246-1251.

(30) Nakatsuji, S.; Matsuda, K.; Uesugi, Y.; Nakashima, K.; Akiyama, S.; Katzer, G.; Fabian, W. *J. Chem. Soc., Perkin Trans. 2* **1991**, 861-867.

(31) Schenk, R.; Gregorius, H.; Meerholz, K.; Heinze, J.; Müllen, K. *J. Am. Chem. Soc.* **1991**, *113*, 2634-2647.

(32) Deb, S. K.; Maddux, T.; Yu, L. *J. Am. Chem. Soc.* **1997**, *119*, 9079-9080.

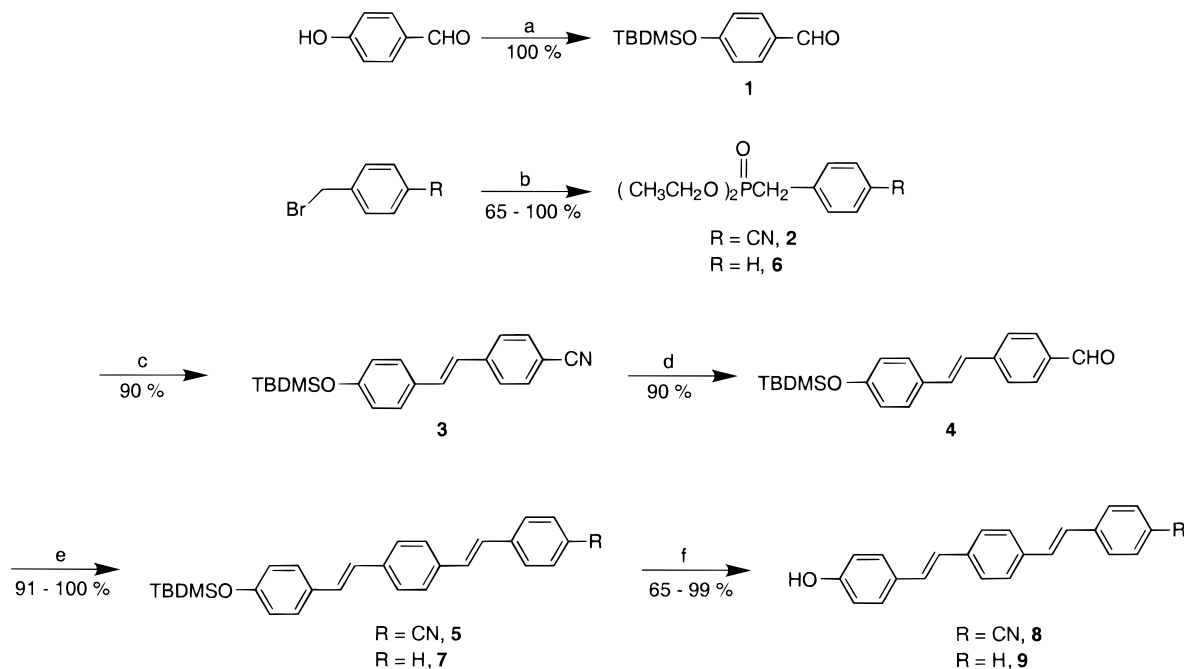
(33) Meier, H.; Lehmann, M. *Angew. Chem., Int. Ed. Engl.* **1998**, *37*, 643-645.

(34) Katz, H. E.; Bent, S. F.; Wilson, W. L.; Schilling, M. L.; Ungashe, S. B. *J. Am. Chem. Soc.* **1994**, *116*, 6631-6635.

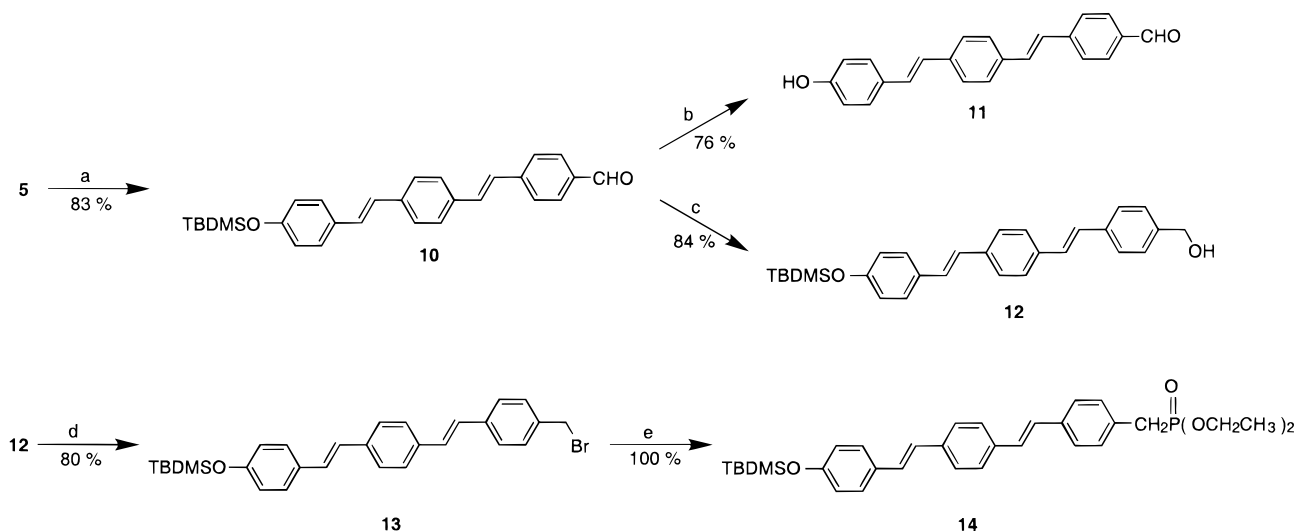
(35) Swzarc, M. *Carbanions, Living Polymers, and Electron-Transfer Processes*; Wiley: New York, 1968.

(36) Morton, M. *Anionic Polymerization: Principles and Practice*; Academic Press: New York, 1983.

(37) Heimenz, P. C. *Polymer Chemistry: The Basic Concepts*; Marcel Dekker: New York, 1984.

Scheme 2^a

^a Reagents: (a) imidazole, *t*-butyldimethylsilylchloride, CH_2Cl_2 , rt, 8 h; (b) triethylphosphite, 140 °C, 4 h; (c) i. 2, LDA, THF, $-78-0$ °C; ii. 1, 0 °C–rt, 8 h; (d) DIBALH, Et_2O , -78 °C, 7 h; (e) i. 2 or 6, LDA, THF, $-78-0$ °C; ii. 4, 0 °C–rt, 8 h; (f) TBAF, THF, rt, 5 min.

Scheme 3^a

^a Reagents: (a) DIBALH, THF, -78 °C, 7 h; (b) TBAF, THF, rt, 5 min; (c) DIBALH, THF, -78 °C, 7 h; (d) NBS, PPh_3 , THF, rt, 3.5 h; (e) triethylphosphite, 140 °C, 4 h.

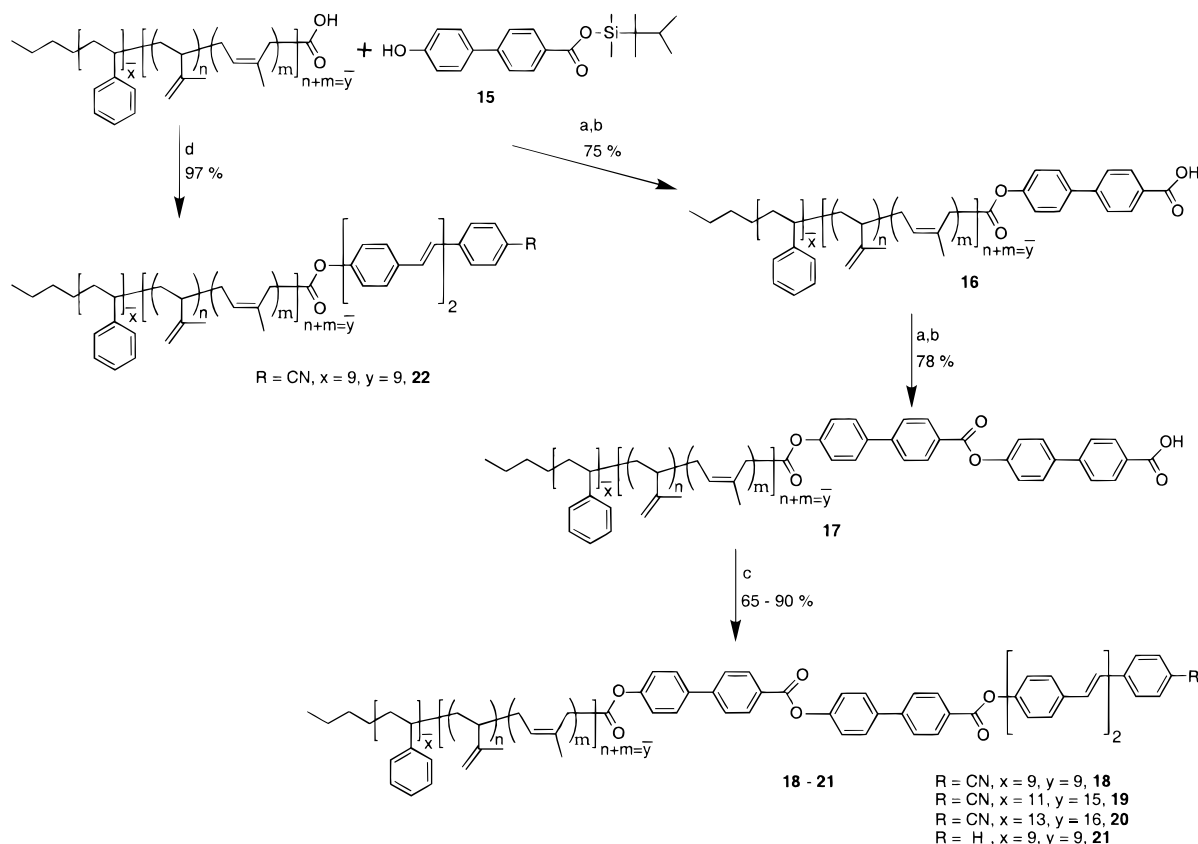
Table 1. Average Number of Styrene and Isoprene Repeat Units Synthesized, the PDI, and the Chemical Functionality of the Diblock Coil Terminus

oligostyrene	oligoisoprene	PDI ^a	coil terminus
9	9	1.09	$-\text{CO}_2\text{H}$
11	15	1.12	$-\text{CO}_2\text{H}$
13	16	1.10	$-\text{CO}_2\text{H}$
11	16	1.06	$-\text{CH}_2\text{CH}_2\text{OH}$

^a Polydispersity index.

weight distribution, a high degree of stereochemical diversity is contained within the molecular backbone of the diblock coil. The styrene block is atactic comprising a random sequence of meso and racemic diads, while the isoprene block contains mostly 1,4 and 3,4 additions but probably has a small amount of 1,2 addition products.

The rod segments of these triblock structures contain either dimers or pentamers of phenylene vinylene. Schemes 2 and 3 outline the synthetic route used to prepare the PV dimers and pentamers. Due to the insolubility of unsubstituted PV oligomers, the direct synthesis of a pentamer rod block is impractical. Our synthetic approach is diverse enough to allow the synthesis of soluble building blocks needed to construct a PV pentamer. For example, **11** can be attached to the diblock coil eliminating insolubility problems prior to pentamer formation. Furthermore our approach, like others in the literature, allows extension of the chemistry to higher molar mass PV oligomers.²³ The two key reactions involved in the synthesis of the PV oligomers are the Horner-Emmons reaction to construct the new vinylene bond and the reduction of the cyano group to an aldehyde for reaction under Horner-Emmons conditions. It was determined

Scheme 4^a

^a Reagents: (a) DIPC, DPTS, CH_2Cl_2 , rt, 8 h; (b) TBAF, THF, -78°C , 4 h; (c) **8** or **9**, DIPC, DPTS, CH_2Cl_2 , rt, 8 h; (d) **8**, DIPC, DPTS, CH_2Cl_2 , rt, 8 h.

experimentally that the highest yields of product were obtained when the phosphonate was precooled to -78°C before addition to the LDA solution already at -78°C . When the phosphonate was precooled, the yield of the desired product ranged from 87 to 98% yield; however, when the phosphonate was added at room temperature to the LDA solution at -78°C , the reaction yields dropped into the 58–75% range. For these lower yielding reactions, no characterizable byproducts could be isolated from the reaction mixture. In general, the reduction of the cyano group with DIBALH in Et_2O gave higher yields but THF is a much better solvent for the PV derivatives. Compound **10** is a key intermediate for PV pentamer synthesis because the silyl group can be easily removed for attachment to the diblock coil or the aldehyde can be further reduced to the benzyl alcohol for eventual transformation to the phosphonate. Standard Arbuzov conditions converted **13** to **14** giving access to **11** and **14**; the two building blocks needed to construct the PV pentamer.

Scheme 4 outlines the series of DPTS/DIPC esterification and silyl deprotection reactions utilized to prepare a variety of triblock molecules containing dimers of PV. On the basis of our understanding of these triblock systems,³ the PV dimers alone would be insufficient to drive the system to nanostructure formation, and this will be shown later in the paper by studying material **22**. For this reason, the rod portion of the molecules was extended by incorporating two biphenyl segments between the diblock coil and the PV dimers. When the silyl deprotection reaction is performed at -78°C , yields range between 88 and 98%; however, if the reaction is allowed to warm much above -78°C , the yields drop into the 65–75% range due to ester bond cleavage. Table 2 summarizes the collection of triblock structures prepared by Scheme 4. Three triblock structures, **18**, **19**, **20**, were prepared with different coil lengths but the same

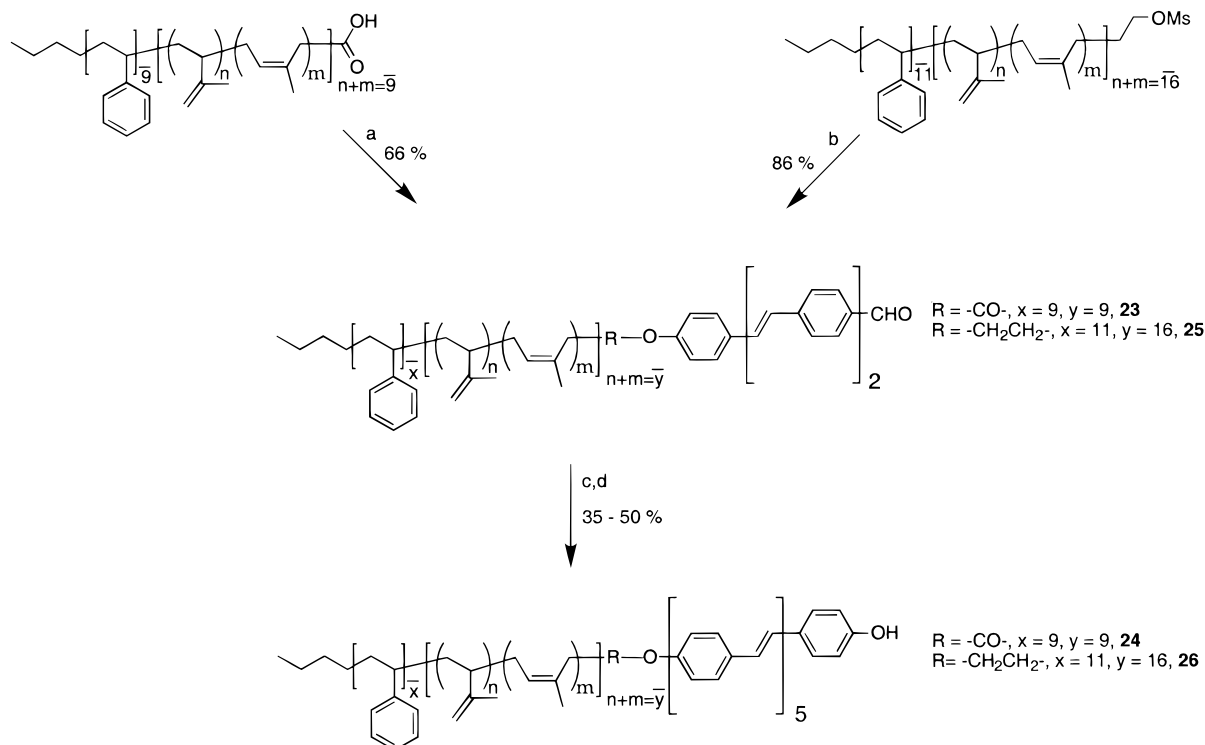
Table 2. Variety of Triblock Rodcoil Molecules Were Prepared: Average Number of Styrene and Isoprene Repeat Units, the Triblock End Group Chemical Functionality, the PDI, and the Compound Number

oligostyrene	oligoisoprene	rod block terminus	PDI ^a	compd
9	9	–CN	1.12	18
11	15	–CN	1.12	19
13	16	–CN	1.08	20
9	9	–H	1.12	21
9	9	–CN	1.11	22

^a Polydispersity index.

rod block. These materials will be referred to by number and coil composition, for example **18** ($\text{Sty}_9\text{,Iso}_9$), when it will help the reader. In addition, the same diblock coil, ($\text{Sty}_9\text{,Iso}_9$), was used to prepare four different triblock structures, **18**, **21**, **22**, and **24**.

Scheme 5 shows the synthesis of two triblock molecules containing PV pentamers. Purification of the reaction mixture following Horner-Emmons coupling of **23** was difficult because the product and impurities have similar retention times on silica gel; therefore, the crude material was treated with TBAF in THF at -78°C . This allows slightly easier separation of the desired product by column chromatography. Compound **24** can be isolated after three silica gel column purifications in 35% yield. There were two reasons for eliminating the carbonyl group within the electronically and optically active triblock molecules containing PV pentamers. As can be seen from Scheme 1, substantially higher yields of the diblock coil were obtained when the reaction was quenched with ethylene oxide gas instead of CO_2 gas. Furthermore, the ester bond at the coil–rod junction has been found to be more thermally labile than the ether bond.³⁸

Scheme 5^a

^a Reagents: (a) **11**, DIPC, DPTS, CH_2Cl_2 , rt, 8 h; (b) Cs_2CO_3 , tetrabutylammonium bromide, THF, reflux, 48 h; (c) i. **14**, LDA, THF, -78°C ; ii. **23** or **25**, -78°C –rt, 8 h; (d) TBAF, THF, -78°C , 4 h.

Using an excess of anhydride (10 equiv) allowed the reaction to proceed to completion so that the starting alcohol could not be detected by ^1H NMR, GPC, or TLC. Similar difficulties in purification were discovered for the synthesis of **26** as were found for **24** but slightly higher yields of 50% were obtained for the two steps.

We were able to prepare triblock rodcoil molecules in which we varied the diblock coil length while keeping the rod portion constant. It was also possible to prepare rodcoil molecules with the same coil but different rod segments. The data obtained from this collection of different molecules has allowed us to elucidate some of the important factors governing self-organizing supramolecular materials from triblock systems. Schemes 4 and 5 contain the collection of triblock rodcoil molecules prepared containing phenylene vinylene rod segments. The supramolecular structures of several of these materials are discussed below.

Supramolecular Film Structure. When solvent cast (0.1 wt % CHCl_3 solution) thin films of **18** ($\text{Sty}_5\text{,Iso}_5$) were investigated by transmission electron microscopy (TEM), small nanosized domains were observed (see Figure 1a). The wide-angle electron diffraction pattern (ED) of the film is also shown in Figure 1c and indicates the presence of crystalline domains. Thus, the areas that appear dark in Figure 1a are believed to result predominately from diffraction contrast and should contain rod blocks which are the only crystallizable segments of **18** ($\text{Sty}_5\text{,Iso}_5$). All TEM micrographs were obtained without the use of stains, and therefore the observed contrast must be due to the presence of crystalline regions. The lighter regions in Figure 1a should contain the amorphous diblock coil segments. The average diameter of the aggregates shown in Figure 1a is roughly 3.5 nm, and the micrograph indicates variation in the size of the nanostructures. In addition, close examination of the micrograph shows small areas where the domains appear to be

strips instead of discrete nanostructures. Interestingly, the ED pattern of **18** ($\text{Sty}_5\text{,Iso}_5$) consists of small arcs, indicating orientation among the nanocrystalline supramolecular units. The origin of this effect is not understood at present but may well arise from shape-related packing effects. It is possible the strip morphology nucleates orientation among nanostructures and this orientation is retained even when the strip morphology breaks up into individual nanostructures. However, there may also be important supramolecular forces leading to this orientation such as the elimination of inplane dipole moments. The ED patterns indicate that rod segments are oriented perpendicular to the plane of the film. Furthermore, the patterns characterize the structure as a 2-D rectangular unit cell containing eight molecules with $a = 18.72 \text{ \AA}$ and $b = 11.10 \text{ \AA}$. Interestingly, when films of **18** ($\text{Sty}_5\text{,Iso}_5$) are annealed near 125°C for several hours, TEM micrographs (see Figure 1b) indicate the average size of supramolecular units increases to roughly 5 nm, and the small strip domains previously observed disappear. Although the average size of the nanostructures increases in diameter, there still appears to be polydispersity in the size of the nanostructures and long-range positional order is not observed among them. However, the ED pattern from the annealed film (Figure 1d) is essentially identical to the ED pattern of the solvent cast film. This indicates that orientation among supramolecular units is preserved despite the observed increase in size and loss of strip-like continuity. The observation of polydispersity in the room-temperature TEM micrographs of **18** ($\text{Sty}_5\text{,Iso}_5$) before and after annealing may result from the systems inability to find one thermodynamically stable aggregate size. The coil length can have a large effect on the systems energy, and we will report later in this paper a system designed to probe the effect of the coils on nanostructure regularity.

Cast films from CHCl_3 solutions of **18** indicate the layer spacing is equal to 6.0 nm and both (001) and (002) reflections

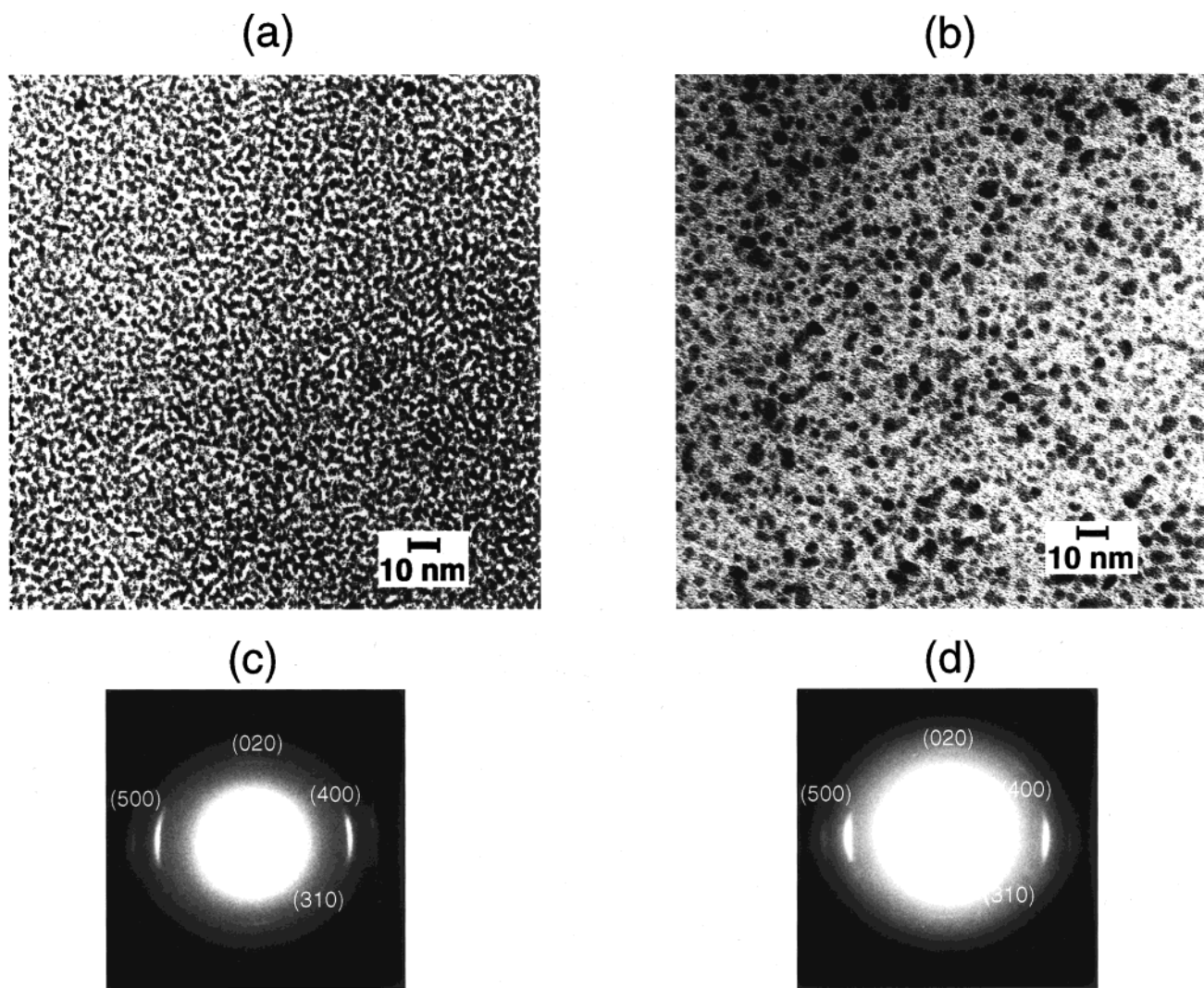


Figure 1. (a) TEM micrograph of a solution cast thin film of **18** ($\text{Sty}_5\text{,Iso}_7$) showing nanostructured aggregates roughly 3.5 nm in diameter. (b) TEM micrograph of an annealed film of **18** ($\text{Sty}_5\text{,Iso}_7$) revealing larger diameter nanostructures. Upon annealing the aggregates increase in diameter to approximately 5 nm. The ED patterns for the solution cast film (c) and the annealed film (d) indicate local supramolecular orientation between individual aggregates. Interestingly, even after annealing the crystallinity and supramolecular orientation remains. All micrographs were obtained without any staining compounds.

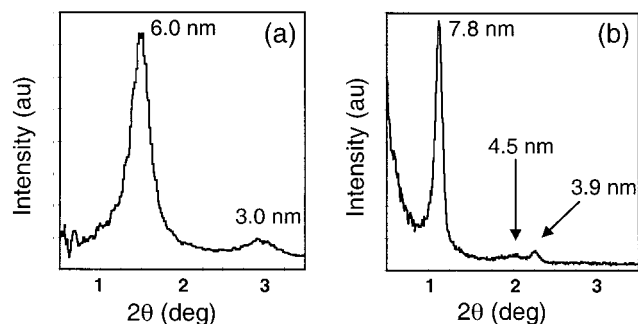


Figure 2. SAXS curves obtained at room temperature of **18** ($\text{Sty}_5\text{,Iso}_7$) as (a) solution cast film and (b) annealed film. After annealing, the layer spacing grows by 18 Å and a new signal at 4.5 nm is observed.

are observed in small-angle X-ray scattering (SAXS) (see Figure 2a). A layer spacing of 6.0 nm is less than the fully extended length of an average sized molecule.³⁹ When the same material was solution cast but annealed at 150 °C for 3–8 h in an N_2 atmosphere and then slow cooled before performing SAXS

measurements, a layer spacing of 7.8 nm was observed as shown in Figure 2b. In addition, a new broad reflection corresponding to a d spacing of 4.5 nm was observed as well. Interestingly, if the annealed material is dissolved and recast the layer spacing reverts back to 6.0 nm, suggesting the aggregates are kinetically trapped in a nonequilibrium size as solvent evaporates. The change in d spacing is not caused by chemical reactions since GPC indicates no change in molecular weight or polydispersity after annealing. Furthermore, when the solvent evaporation rate was reduced by saturating the atmosphere with solvent, the layer spacing measured by SAXS is 7.2 nm. This temperature-dependent behavior may be related to the presence of solvent in the originally cast films.

Steric forces are believed to play an important role in nanostructure formation.³ If diblock coil segments are still solvated as rod blocks crystallize, the steric forces among coil segments would be greater. This increase in steric repulsion could stabilize smaller nanostructures if the coils entropy limits their growth. Even if the solvent finally evaporates, the smaller aggregates would be trapped because the material is glassy at 25 °C. When the material is annealed at 150 °C, much less solvent is present, and the lower enthalpy associated with further

(39) SYBYL, Version 6.1, Tripos Associates, St. Louis MO.

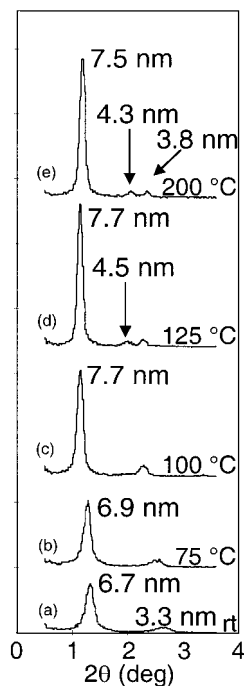


Figure 3. VT-SAXS curves for **18** ($\text{Sty}_5, \text{Iso}_5$) show how the layer spacing increases gradually with increasing temperature. The new peak at 4.5 nm at 125 °C may be related to ordering among supramolecular units at elevated temperature. These materials remain ordered at high temperature as demonstrated by the curve at 200 °C. The changes in d-spacing are irreversible.

rod segment crystallization must be the controlling thermodynamic factor. The 18 Å change in layer spacing after annealing is quite remarkable and would be consistent with an increase in the diameter of the supramolecular nanostructures as observed by TEM. As the diameter of the nanostructure increases, more coils are incorporated in the aggregate which requires the flexible coils toward the interior of the aggregate to stretch out. This stretching of the interior coils would be reflected in an increase in layer spacing observed with SAXS.

Variable-temperature SAXS experiments were performed to further investigate the change in layer spacing observed for **18** ($\text{Sty}_5, \text{Iso}_5$) (several curves are shown in Figure 3). Interestingly, the room-temperature curve for **18** ($\text{Sty}_5, \text{Iso}_5$) shows a layer spacing of 6.7 nm; this sample was solution cast and stored at -10 °C four months prior to SAXS characterization. This slow increase in layer spacing further supports the possibility that this material is initially kinetically trapped into 6.0 nm tall clusters. The bottom three curves demonstrate how the layer spacing increases as the temperature is increased. At 100 °C, the layer spacing has reached its maximum of 7.7 nm, and further annealing does not result in greater layer spacing increases. When the temperature is increased to 125 °C, the peak near 4.5 nm is observed in the X-ray scan (see Figure 2b). The top scan in Figure 3, obtained at 200 °C, demonstrates the strong tendency of this system to order.

The broad peak corresponding to a 4.5 nm d spacing is believed to result from periodic 2-D positional ordering of the larger supramolecular nanostructures observed by TEM. If the nanostructures were sufficiently organized, one could expect the observed peak. The peak positions in SAXS scans shown in Figures 2b, 3d, and 3e could be consistent with a hexagonal lattice because the ratio between the first and second peaks is the square root of 3. However, we do not believe this system has a phase transition from lamellar to hexagonal near 125 °C

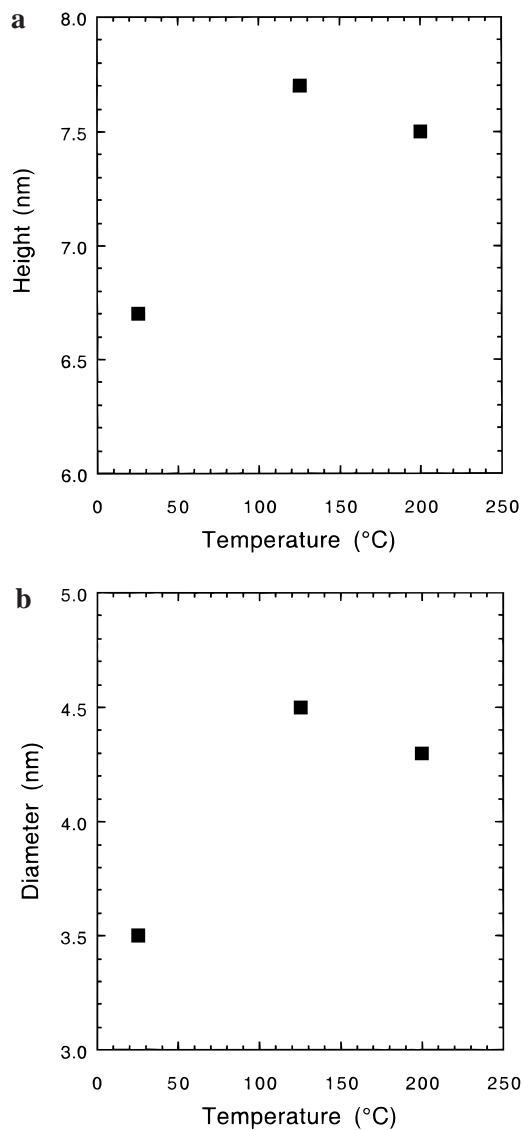


Figure 4. (a) Height and (b) diameter change of the nanostructures is plotted versus temperature. The height data is taken directly from Figure 3 as are the two data points for the diameter at 4.5 and 4.3 nm. Data point 3.5 nm for the diameter is taken from the TEM micrograph of Figure 1a. The synchronized changes in height and diameter are consistent with the model describing the growth of these nanostructures.

since upon slow cooling to room temperature over approximately 8 h the SAXS patterns remain identical, and thus the observed changes are irreversible. Once samples are heated and then cooled, they retain a spacing of 7.8 nm as opposed to the original value of 6.7 nm (see Figure 3). Also, if a transition were to occur from a lamellar to a hexagonal phase, one would expect a change in primary spacing. A hexagonal phase of cylinders would be expected to give rise to a more ordered structure than is observed by TEM for the material after heating (see Figure 1b). Furthermore, cross-sectional analysis by electron microscopy of these supramolecular films confirm the presence of a lamellar phase even after annealing.⁴⁰ The breadth of the peak at 4.5 nm as shown in Figures 2b and 3d may result from the absence of 3-D order among the nanostructures. In fact, similar observations were found in layered DNA–lipid phases where the (001) reflections from lipid bilayers are observed along with a characteristically broader reflection associated with 2-D ordering of DNA chains lacking 3-D correlation.^{41,42}

(40) Pralle, M. U.; Tew, G. N.; Stupp, S. I., manuscript in preparation.

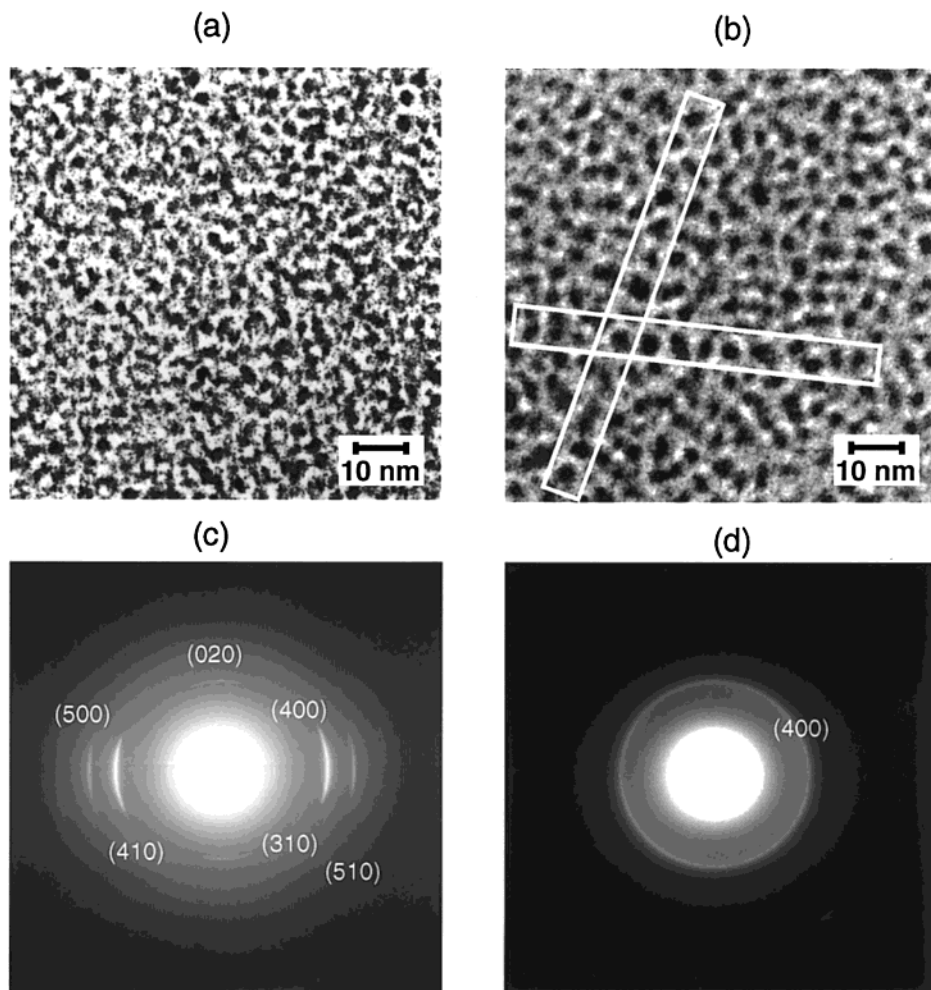


Figure 5. Direct TEM comparison of the nanostructures formed by (a) **18** ($\text{Sty}_{11},\text{Iso}_{15}$) and (b) **19** ($\text{Sty}_5,\text{Iso}_5$). The diblock coil has a substantial effect on the size and regularity of the nanostructures. The ED patterns from the two materials are also different. Films of (c) **18** ($\text{Sty}_5,\text{Iso}_5$) are highly crystalline and highly oriented, while (d) **19** ($\text{Sty}_{11},\text{Iso}_{15}$) is less crystalline and less oriented. However, the brightest reflections come at exactly the same spacing in both materials, suggesting the rods pack into the same structure.

Interestingly, the layered d spacing reflection observed by SAXS for **18** is rather sharp indicating an ordered layered system but TEM micrographs shown in Figure 1 reveal inter-cluster disorder in the x - y plane. Thus, the apparent 2-D disorder among supramolecular aggregates does not affect the system's ability to order into well-defined layers as indicated by SAXS. This is analogous to the nature of order observed in a classical smectic-A phase in which a characteristic spacing is observed as a result of molecular layering. However, each layer is essentially a 2-D liquid. In our system the supramolecular clusters are equivalent to smectogens in the classical phase, and layering occurs easily because clusters are monodisperse in height. In a classical smectic-A phase on the other hand, the molecule's molar mass is the monodisperse element leading to defined layering. Therefore, in our systems the nanostructures defined by crystallization of rod segments are driven to organize into discrete layers whether the nanostructures are polydisperse or monodisperse, and whether or not the nanostructures are organized into a 2-D lattice.

The reflection corresponding to 4.5 nm shown in Figure 2b is broader at room temperature suggesting that x - y ordering of the nanostructures may improve at elevated temperature (see

Figure 3d,e). It is possible that at elevated temperatures the size, shape, and dimension of the nanostructures is more regular and this regularity leads to increased positional order. Furthermore, at elevated temperature it is likely that the coils explore more conformations, perhaps leading to more regularly shaped nanostructures. The changes in height and diameter of the nanostructures as a function of temperature are shown in Figure 4a and b. The graphs show clearly that the changes in height and diameter of the nanostructures are correlated. These synchronized changes support further the suggestion that more molecules pack into a single nanostructure as the kinetic conditions are replaced by thermodynamic energies. A larger molecular aggregate would be expected to result in nanostructures of greater height as a result of stretching of coil segments in their interior as mentioned earlier. The observation of a plateau in height and diameter must be related to the thermodynamics of the system which prefers to form aggregates of a specific size. One approach to mimicking the coils entropy at elevated temperatures is to lengthen the coil segments as we did in preparing **19** ($\text{Sty}_{11},\text{Iso}_{15}$).

To further investigate the rules leading to regularly shaped nanostructures, we prepared **19** ($\text{Sty}_{11},\text{Iso}_{15}$) which possesses an identical rod segment as **18** ($\text{Sty}_5,\text{Iso}_5$) but a longer coil. Another report from our laboratory suggested rod-coil volume fractions are important to nanostructure dimensions and regular-

(41) Salditt, T.; Koltover, I.; Rädler, J. O.; Safinya, C. R. *Phys. Rev. E* **1998**, *58*, 889–904.

(42) O'Hern, C. S.; Lubensky, T. C. *Phys. Rev. Lett.* **1998**, *80*, 4345–4348.

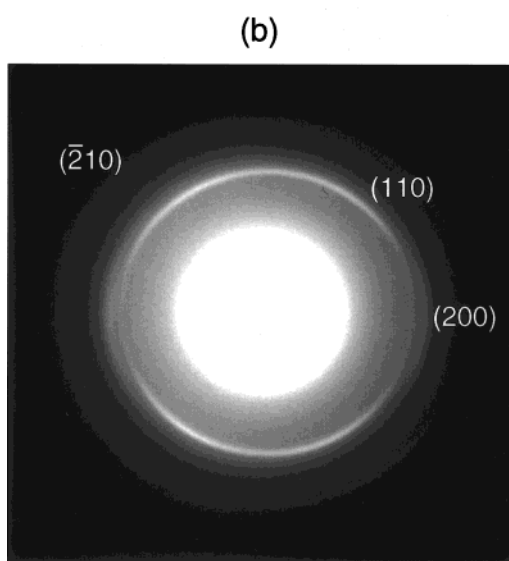
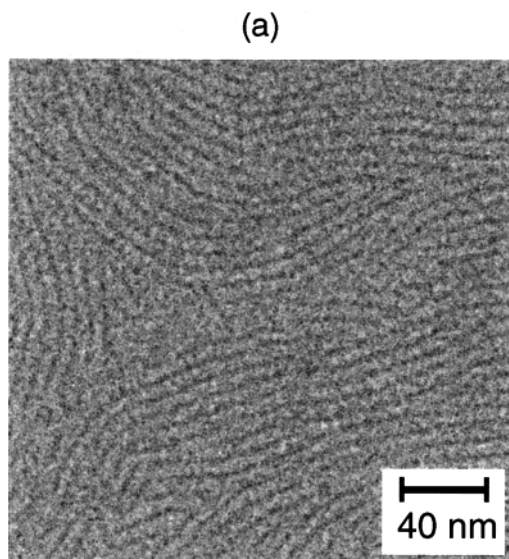


Figure 6. (a) TEM micrograph of **26** revealing the formation of strips with nanoscale dimensions. The strips are 8 nm in width and approximately 80 nm in length, and rod segments are perpendicular to the plane of the micrograph. (b) ED determines the crystal structure of the rods to match closely that of the polymer poly(*p*-phenylene vinylene). The unit cell for the rods is characterized as $a = 7.95 \text{ \AA}$ and $b = 5.15 \text{ \AA}$. This material displays orientation in the ED pattern and could be expected given the presence of strips.

ity.⁴³ Comparison of TEM micrographs obtained for films of **18** ($\text{Sty}_{\bar{9}}, \text{Iso}_{\bar{9}}$) and **19** ($\text{Sty}_{\bar{11}}, \text{Iso}_{\bar{15}}$) indeed reveals that the nature of the coil can have a major impact on the polydispersity of nanostructure size. The nanostructures formed by **19** ($\text{Sty}_{\bar{11}}, \text{Iso}_{\bar{15}}$) in Figure 5b are more regular in size with sharply defined boundaries and more circular 2-D projections compared to **18** ($\text{Sty}_{\bar{9}}, \text{Iso}_{\bar{9}}$) in Figure 5a. Furthermore, two boxes are shown in 5b which clearly depict the longer range positional order observed in films of **19** ($\text{Sty}_{\bar{11}}, \text{Iso}_{\bar{15}}$). The reason for longer range positional ordering is probably the result of a narrower polydispersity in dimensions between the aggregates. Interestingly, this narrowing of distribution may be related to larger entropic contributions from the longer coils thus allowing the system to explore more conformations at room temperature

(43) Pralle, M. U.; Whitaker, C. M.; Braun, P. V.; Stupp, S. I., manuscript in preparation.

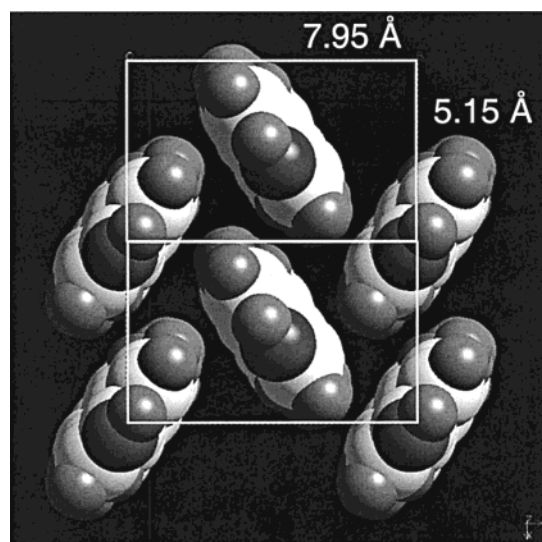


Figure 7. Molecular graphics model showing the herringbone packing of the phenylene vinylene oligomeric rods. These rods pack in a fashion very similar to that of the polymer PPV. Interestingly, the unit cell for these rods is noncentrosymmetric. A noncentrosymmetric rod crystallite would be required for these materials to exhibit polar stacking.^{3,17}

leading to similarly sized nanostructures. The SAXS scans of **19** ($\text{Sty}_{\bar{11}}, \text{Iso}_{\bar{15}}$) indicate a d spacing of 8.0 nm corresponding to the height of nanostructures and this spacing is consistent with the size of the aggregates and the coil length. As expected, the spacing of 8.0 nm for **19** ($\text{Sty}_{\bar{11}}, \text{Iso}_{\bar{15}}$) is slightly larger than 7.8 nm found for **18** ($\text{Sty}_{\bar{9}}, \text{Iso}_{\bar{9}}$).

Comparison of the ED patterns from **18** ($\text{Sty}_{\bar{9}}, \text{Iso}_{\bar{9}}$) and **19** ($\text{Sty}_{\bar{11}}, \text{Iso}_{\bar{15}}$) show the most intense reflections match exactly suggesting the rod portions of the two molecules crystallize into the same structure. ED of **19** ($\text{Sty}_{\bar{11}}, \text{Iso}_{\bar{15}}$) has fewer reflections than **18** ($\text{Sty}_{\bar{9}}, \text{Iso}_{\bar{9}}$) and this is most likely due to a less ordered rod cluster as a result of longer coil segments. There is more orientational order among nanostructures in **18** ($\text{Sty}_{\bar{9}}, \text{Iso}_{\bar{9}}$) as indicated by the arcs vs Debye rings nature of the ED patterns. If the orientation in the ED pattern is connected to the strip-like morphologies observed by TEM, then it is not surprising that **19** ($\text{Sty}_{\bar{11}}, \text{Iso}_{\bar{15}}$) exhibits a lower degree of orientation.

The design of molecule **26** was conceived to combine the photonic properties of PPV with the nanostructured morphology of aggregated rodcoil molecules. SAXS measurements of this material gave a reflection corresponding to a d spacing of 8.5 nm, again less than the extended molecular length, suggesting a monolayered packing arrangement and mushroom as opposed to dumbbell supramolecular architecture. The electron micrograph in Figure 6a shows this system does indeed nanophase separate. However, the nanostructures have a high aspect ratio near 10. The objects are spaced 8 nm from center to center in the micrograph and average about 80 nm in length. This strip structure is the most likely organization because the ED pattern characterizes the rod segments to be perpendicular to the plane of the film. These nanostructures are different from the mushroom nanostructure and similar structures have been previously observed in our laboratory.¹⁶ Our previous work showed that diblock rodcoils could self-assemble into strip phases as well as discrete nanostructured phases simply by varying the rod vs coil volume fraction. Although we do not fully understand the strip morphology, it may be related to the fusing of nanostructures. Because the rod segments in **26** are longer than previous rod segments, they may have a lower enthalpy of aggregation which would lead to larger diameter

nanostructures. However, the formation of larger nanostructures requires more coil segments to be trapped in the middle of aggregates costing a larger entropic penalty. A compromise between enthalpy and entropy could be the formation of strips where fewer coil segments are segregated to the interior yet more rod segments are packed into the nano-crystal.

The ED pattern in Figure 6b is an a^*b^* diffraction plane of a 2-D rectangular lattice revealing some preferred orientation. The observed lattice orientation may be linked to the strip morphology observed in the TEM image in Figure 6a as previously suggested. The spacings corresponding to the observed reflections closely match those observed for the polymer PPV.⁴⁴ The a and b lattice parameters measured are 7.95 and 5.15 Å, respectively; both values are 0.05 Å larger than those reported in the literature for the polymer. Considering the similarity in lattice parameters between **26** and the polymer, it is reasonable to assume the oligomers pack into the same structure as the polymer. To verify this, a model of the crystal structure was generated with Cerius² using the measured spacings.⁴⁵ This model was then energy minimized resulting in the structure shown in Figure 7 which has the same herringbone packing as the polymer. In this configuration, one may infer the rod segments are oriented perpendicular to the film. Another interesting feature of this crystal packing model is the polar nature of the structure. To generate the herringbone structure shown, two molecules make up the unit cell with one molecule at the (0,0,0) position and the other molecule at the (1/2,1/2,0) position. Interestingly, this results in a noncentrosymmetric crystal due to the presence of dissimilar end groups in oligomer molecules. The formation of a polar crystal is not surprising, given that we have found evidence for polar order in a variety of rodcoil materials, all of which have SAXS reflections consistent with monolayer formation.^{3,17} To create a centrosymmetric crystal, molecules would either have to interdigitate or align end-to-end forming a dumbbell-shaped aggregate where coil segments extend from the top and bottom of the supramolecular aggregate. However, SAXS measurements indicate this is not the case because the observed layer spacing is less than one fully extended molecule. This is strong evidence against the formation of bilayers in these materials.

TEM micrographs of **21** (not shown) revealed similar images to those shown in Figure 1a with a large polydispersity in aggregate size and no apparent positional ordering. Likewise, SAXS scans of solution cast films of **21** also show a layer spacing that increases with annealing time from 7.2 to 7.7 nm (150 °C, 3–8 h, N₂). Samples **22** and **23** do not show any ordering at the nanostructure level. These materials form glassy solids at room temperature that are not birefringent when viewed between cross polars in an optical microscope. At the same time SAXS scans do not reveal any peaks for samples **22** and **23** and ED reveals no diffraction for **22** indeed supporting the suggestion that these small PV dimers cannot drive nanostructure formation. The high degree of self-organization in **18**, **19**, **21**, **26** and other triblock rodcoil molecules synthesized in our laboratory⁴³ and the lack of any order in **22** and **23** suggest that rod-to-coil volume ratio is indeed a key variable in the self-assembly of these block molecules. Furthermore, coil-to-rod volume fraction can have a strong effect on nanostructure size distribution as demonstrated by electron microscopy of **18** and **19**. Polydisperse nanostructures were observed when the coil was shorter and this effect could be related to the relative weight

of enthalpic and entropic effects on nanostructure formation. This effect could also be explained partly by differences in coil segment structure in both samples. The strip morphology observed in **26** is possibly the result of a more favorable enthalpy of aggregation for oligo-*p*-phenylene vinylene rod segments relative to those in **18** and **19**, and this particular shape should be entropically more favorable given the greater number of peripheral rodcoil molecules relative to round nanostructures.

Absorption and Fluorescence. Figure 8a shows the absorption spectra for **8** along with absorption and fluorescence spectra for **18** in solution. The absorption spectrum for **8** reveals a maximum at 378 nm and a peak shape with less vibronic structure than most laterally unsubstituted PV oligomers.^{34,46} This may result from the large push–pull character of **8**. When **8** is incorporated into the rodcoil, **18**, a slight blue-shift (9 nm) was observed which is expected because the chromophore is attached through the free phenol in **8** to an ester function in the triblock structure. The solution emission spectrum of **18** is broad with a maximum at 446 nm, corresponding to blue light emission upon excitation. Figure 8b shows both the absorption and emission spectra for **18** as a dilute solution and solid film. Interestingly, the absorption spectra corresponding to the dilute solution and solid film almost exactly overlap with only a relatively small blue shift of 9 nm observed for the maxima. A similar small shift is observed in the emission spectra; the emission profile of solid **18** is narrower and red shifted by only 10 nm relative to that of the dilute solution. The red-shift in solid-state emission is smaller than other similar compounds reported in the literature,^{34,46} while the decrease in width of the emission in the solid state is not typically observed. Furthermore when the dilute solution and solid films of **22** were studied as non-nanostructured control samples, the absorption and emission spectra were found to be more similar to those of other reported PV-based materials. These spectra are shown in Figure 8c. The solid films show significantly blue shifted absorption (31 nm) and red shifted emission (26 nm) maxima. Films of **22** were found to be amorphous by ED and contain no ordering as determined by SAXS and optical microscopy.

There is a clear difference in the absorption and emission profiles for the supramolecular film of **18** and the unordered film of **22**. Both theoretical⁴⁷ and experimental⁴⁸ reports in the literature suggest small aggregates from two to six stilbene molecules can alter the absorption and fluorescence spectra of the isolated chromophore leading to blue shifted absorption and red shifted emission. This molecular aggregation is typically an H-aggregate where the long axes of the molecules are aligned parallel to each other. In addition, Brédas⁴⁷ and co-workers have shown theoretically that the angle between the long molecular axes of neighboring chromophores can have a dramatic effect on absorption and emission profiles, as well as luminescence efficiency. They reported that as the angle is increased, the splitting between the lowest optical transitions is decreased leading to a blue shifted absorption. TEM data discussed previously for the supramolecular material, **18**, suggests there are roughly 60–80 molecules per nanostructure. Regardless of the exact number of molecules in the aggregates, the nanostructures contain many more molecules than the two to six molecules shown to produce changes in their spectra. Laterally unsubstituted oligomers of PV have been investigated both in

(44) Granier, T.; Thomas, E. L.; Gagnon, D. R.; Karasz, F. E.; Lenz, R. W. *J. Polym. Sci. Part B: Polym. Phys.* **1986**, *24*, 2793–2804.

(45) Cerius²-molecular graphics program from Molecular Simulations, Inc.

(46) Oelkrug, D.; Tompert, A.; Egelhaaf, H.-J.; Hanack, M.; Steinhuber, E.; Hohloch, M.; Meier, H.; Stalmack, U. *Synth. Met.* **1996**, *83*, 231–237.

(47) Cornil, J.; dos Santos, D. A.; Crispin, X.; Silbey, R.; Brédas, J. L. *J. Am. Chem. Soc.* **1998**, *120*, 1289–1299.

(48) Song, X.; Geiger, C.; Farahat, M.; Perlstien, J.; Whitten, D. G. *J. Am. Chem. Soc.* **1997**, *119*, 12481–12491.

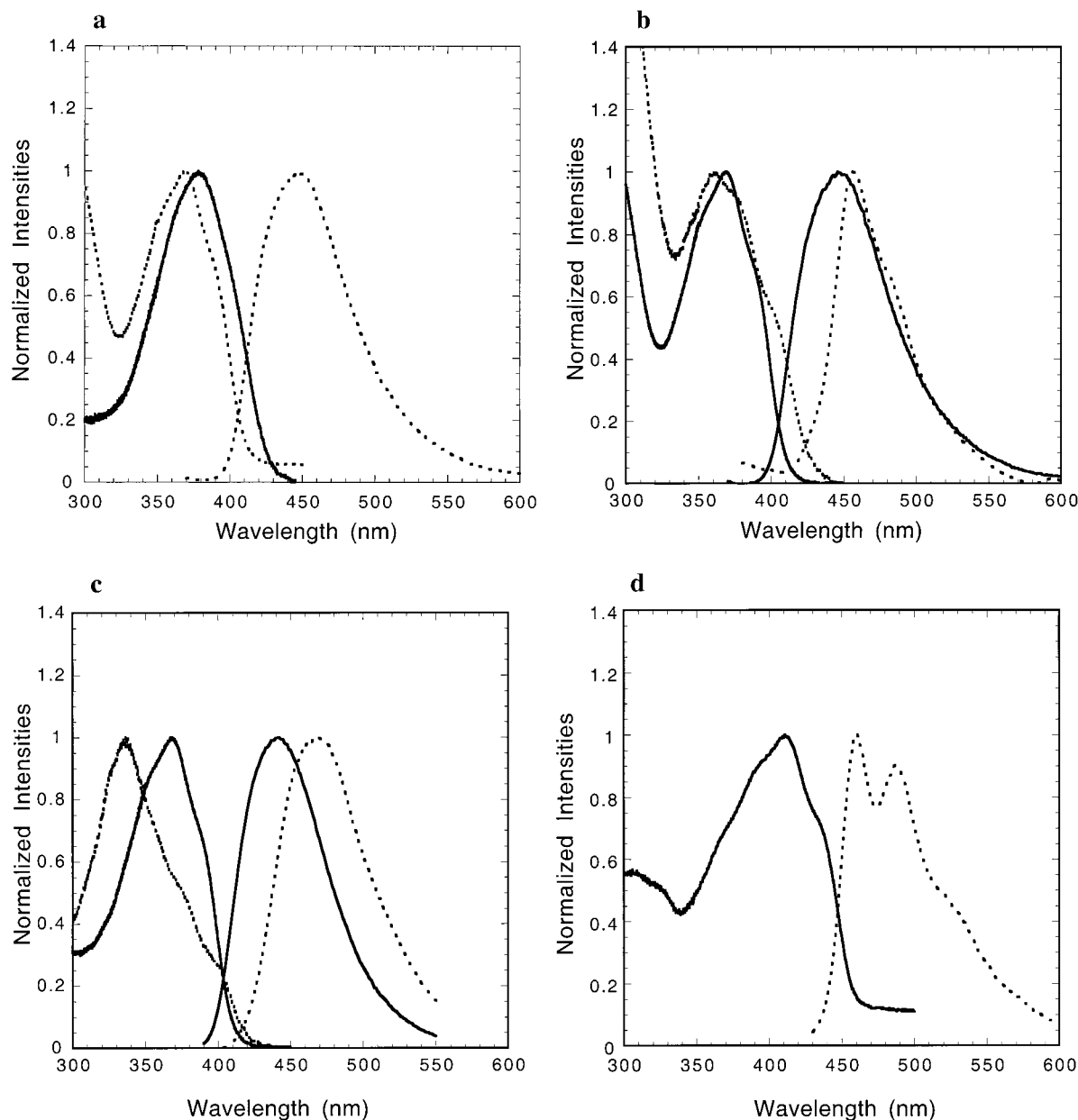


Figure 8. (a) Absorption spectra are shown for two samples; **8** (solid) which has $\lambda_{\text{max}} = 378$ nm and **18** (dotted) has $\lambda_{\text{max}} = 369$ nm. The spectra were collected in THF with optical density near 0.1. The fluorescence emission of **18** from dilute solutions in THF has $\lambda_{\text{max}} = 446$ nm with the excitation wavelength of 331 nm. (b) Absorption and emission spectra are shown for both solution (solid) and solid film (dotted) of **18**. A small blue-shift (9 nm) in the absorbance and red-shift (10 nm) in the emission are observed between the solution and solid samples. (c) A similar set of spectra to 8b are shown for **22** with solution (solid) and film (dotted) spectra compared to each other. These spectra show larger shifts than those of the nanostructured material **18** and more typical of laterally unsubstituted PV chromophores. The films of **22** are amorphous from ED, SAXS, and optical microscopy. (d) Solution absorption and emission from **26** has an absorption $\lambda_{\text{max}} = 411$ nm and emission maxima at 461 and 487 nm. The excitation wavelength for the emission spectra was 410 nm.

solution and in the solid state.^{34,46} Both distyrylbenzene and 1,4-Bis(3,5-di-*tert*-butylstyryl)benzene show blue-shifted absorption and red-shifted emission in the solid state.⁴⁶ However, the absorption and emission spectra of the *tert*-butyl analogue are shifted less than those of distyrylbenzene. These smaller shifts are explained by the presence of bulky substituents that reduce band splitting.⁴⁶ Therefore, we could expect similar small shifts in both absorption and emission for **18** and **22** since PV oligomers are attached to a very bulky diblock coil. However, this explanation fails to explain the differences in the magnitudes of the shifts between peaks shown in Figure 8b and 8c or the narrowing of emission shown in Figure 8b. In both cases, alignment of the long molecular axis is probably close to a H-type aggregate especially the non-nanostructured material (see

Figure 8c). It is likely that the observed spectra for the supramolecular film are a result of more specific packing modes among chromophores within the nanostructures. One possibility is that within nanostructure the chromophores are actually ordered into smaller domains that cannot be observed by TEM or ED. This additional ordering within the nanostructure could produce smaller aggregates on the order of two to six molecules, thus resulting in the observed spectra. It is also possible that the angle between the PV chromophores within the rod segments of the aggregate is nonzero, therefore producing solid-state spectra that resemble dilute solution. Alignment of the PV chromophores within the aggregate should not be confused with the nanostructure positional ordering discussed earlier. The red-shifted absorption and emission spectra of **26** relative to **18**

shown in Figure 8d are expected due to increased conjugation along the molecular backbone and are typically of PV pentamers.

Conclusions

The formation of supramolecular nanostructures and hierarchical order in materials formed by rodcoil molecules can be completely suppressed by a lower rod-to-coil volume ratio. When the chemical structure of rod segments is changed, the nanostructures formed can increase drastically in aspect ratio. These changes in shape may be linked to different tendencies for aggregation among rod segments. At the same time, the ratio of rod vs coil volume fraction can have a large impact on the polydispersity of the nanostructures formed.

Experimental Section

General. Unless otherwise noted, all starting materials were obtained from commercial suppliers and used without further purification. CH_2Cl_2 was distilled over CaH_2 prior to use. THF, Et_2O , toluene, and benzene were distilled from Na^0 /benzophenone. 1,3-Diisopropyl carbodiimide (DIPC) was distilled prior to use, and 4-(dimethylamino)pyridinium-4-toluenesulfonate (DPTS) was prepared according to literature.⁴⁴ Styrene and isoprene were vacuum transferred from CaH_2 after washing to remove inhibitor. MgSO_4 was used to dry all organic solutions during workup procedures. Analytical thin-layer chromatography (TLC) was performed on KIESELGEL F-254 precoated TLC plates. Silica for flash chromatography was silica gel 60 (230–400 mesh) from EM Science. The ^1H NMR and ^{13}C NMR spectra were recorded on a GE 300, Varian Unity 400, or Unity 500 spectrometer. Chemical shifts are expressed in parts per million (δ) using residual solvent protons or TMS as internal standard. Mass spectrometry was performed by the Mass Spectroscopy Laboratory at the University of Illinois. Low-resolution mass spectra were obtained on a Finnigan-MAT CH5 spectrometer operating at 70 eV. High-resolution electron impact mass spectra were obtained on a Finnigan-MAT 731 spectrometer operating at 70 eV. Low- and high-resolution fast atom bombardment (FAB) mass spectra were obtained on VG ZAB-SE and VG 70-SE-4F spectrometers. Matrix-assisted laser desorption ionization (MALDI) mass spectra were obtained on a VG TofSpec spectrometer. Elemental analysis was performed by the University of Illinois Micro analytical Service Laboratory using a Perkin-Elmer model P2000 analyzer. Gel permeation chromatography (GPC) was performed with Waters styragel HMW 2 and styragel HMW 6E columns, 510 pumps, 486 UV-detector, and 410 RI detector using THF as mobile phase. Small-angle X-ray studies were carried out on a Siemens Anton Paar high-resolution small angle camera equipped with a Hi-Star area detector and Siemens SAXS software mounted on an M18X-HF22 SRA rotating anode generator. Powder diffraction rings were integrated over 360° to yield the diffraction patterns, and the system was calibrated using a silver behenate standard. Transmission electron microscopy studies were performed on a Phillips CM 200 TEM operating at 120 keV accelerating voltage. Solution cast samples were prepared by casting from a chloroform solution (0.1 wt %) onto a water surface and then transferring the resulting films to copper TEM grids. Annealed samples were cast from chloroform (0.1 wt %) onto glycerin and annealed at 125°C and then washed in water and transferred to copper TEM grids. Electron diffraction patterns were calibrated with a gold standard. The UV-vis absorption spectra were recorded on a Shimadzu (model UV-160A) spectrophotometer using 1-cm quartz cells and THF as solvent. The fluorescence spectra were recorded on a Photon Technology International (PTI) QM-1 fluorometer. The optical densities of the solutions were between 0.85 and 0.12 at the excitation wavelengths, and THF was the solvent. Films were solution cast and annealed before fluorescence measurements. All emission spectra were recorded in the right angle geometry at room temperature, and thin films were collected using the front face geometry.

General Method for Arbusov reaction.⁴⁹ Equal molar amounts of the benzyl bromide (5.0 g, 29.2 mmol, 1equiv) and triethyl phosphite

(4.81 mL, 29.2 mmol, 1equiv) were placed in a flask with a magnetic stirring bar. A distillation apparatus with thermometer was attached, and the entire system back-filled with N_2 . The slurry was immersed in an oil bath at 70°C with stirring. The oil bath was heated to $130\text{--}140^\circ\text{C}$ and the reaction stirred for 4 h. Ethyl bromide was collected and the reaction stopped when ethyl bromide evolution ceased. The reaction mixture was cooled, diluted with Et_2O , and washed with H_2O and twice with saturated aqueous NaHCO_3 . The organic layer was dried, filtered, and concentrated in vacuo. The resulting oil was immediately purified by flash chromatography on silica gel, using $\text{EtOAc}/\text{CH}_2\text{Cl}_2$ as eluant, affording 70% yield of the desired phosphonate (4.5 g). Phosphonates were used immediately due to decreasing yields of the Horner-Emmons reaction after storage.

General Method for the Horner-Emmons reaction.⁵⁰ All glassware was oven-dried and cooled under N_2 . Diisopropylamine (1.79 mL, 12.8 mmol, 2.5 equiv) was added followed by THF (typically 0.5 M) and the solution cooled to -78°C in a dry ice/acetone bath. *n*-BuLi (7.0 mL, 11.2 mmol, 2.2 equiv, 1.6 M in hexane) was added via syringe, and the mixture was warmed to 0°C for 30 min and then recooled to -78°C . The phosphonate (1.3 g, 5.1 mmol, 1.0 equiv) as a THF solution (typically 0.4 M) was precooled to -78°C and transferred via cannula into the LDA solution. The reaction was placed in a 0°C ice bath and the aldehyde (1.73 g, 5.1 mmol, 1.0 equiv) as a THF solution (typically 0.4 M) was cannulated into the mixture and the ice bath was removed. The reaction was stirred overnight at room temperature. The solution was diluted with CH_2Cl_2 and washed with saturated aqueous NaHCO_3 twice followed by saturated aqueous NaCl . The organic layer was collected, dried, filtered, and concentrated in vacuo. The desired product was recrystallized from the reaction mixture using $\text{CH}_2\text{Cl}_2/\text{Et}_2\text{O}$ to give the all-*trans* product in quantitative yield.

General Method for the Esterification of Carboxylic Acids. The acid (0.300 g, 0.2 mmol, 1 equiv), alcohol (0.058 g, 0.2 mmol, 1 equiv), DPTS (0.052 g, 0.2 mmol, 1 equiv), and CH_2Cl_2 (30 mL) were all combined in an oven-dried flask with stirring bar under N_2 . This produced a turbid solution due to the insolubility of the phenol. DIPC (0.08 mL, 0.6 mmol, 3 equiv) was added via syringe, and the reaction was allowed to stir for 24 h. The reaction was diluted with CH_2Cl_2 and washed twice with H_2O . The organic layer was collected, dried, filtered, and concentrated in vacuo. The product was isolated by flash chromatography ($\text{SiO}_2/\text{CH}_2\text{Cl}_2$). Urea impurities were easily removed by dissolving the solid in CH_2Cl_2 and precipitating into MeOH affording 0.235 g of the desired product (66% yield).

General Method for the Silyl Deprotection of Biphenyl Derivatives. The protected rodcoil (1.20 g, 0.3 mmol, 1.0 equiv) was taken up in THF (0.1 M) and cooled to -78°C . TBAF (2.65 mL, 2.65 mmol, 9 equiv, 1.0 M in THF) was added via syringe in two portions. Three-quarters of the TBAF were added and the reaction was stirred for 3 h at -78°C , then the remaining TBAF was added followed by stirring for 1 h at -78°C . The reaction was quenched with 3 mL of 10% AcOH/THF . The reaction was diluted with CH_2Cl_2 and washed with H_2O . The organic layer was collected, dried, filtered, and concentrated in vacuo. Flash chromatography using CH_2Cl_2 as the eluant afforded 1.1 g of pure material (98% yield).

General Diblock Oligo(X)styrene-*b*-oligo(Y)isoprene Coil Synthesis. Fifty milliliters of benzene and 5 mL of THF were placed in a flask, *n*-BuLi (3.9 mL, 6.24 mmol, 1.0 equiv, 1.6 M) was added, followed by the addition of styrene (5 mL, 43.7 mmol, 9.0 equiv). The reaction was stirred for 30 min. Isoprene (4.37 mL, 43.7 mmol, 9.0 equiv) was added, the reaction stirred for an additional 30 min, and was then quenched by bubbling dry CO_2 through the solution followed by 3 mL of 6 N HCl/THF (1/5).^{51,52} The solvent was removed by rotatory evaporation. The crude material was loaded onto 300 mL of silica gel using CH_2Cl_2 as the solvent. Next, 1500 mL of CH_2Cl_2 was eluted through the column, followed by 1500 mL of acetone. The acetone was evaporated by rotatory evaporation to afford a white tacky glass (1.6 g, 17%). ^1H NMR (400 MHz, CDCl_3) δ 7.00 (br m, 46H), 4.64 (br m, 11H), 3.30 (br m, 2H), 1.40 (br m, 100H); GPC (254 nm,

(50) Wadsworth, W. *Org. React.* **1977**, 25, 73–253.

(51) Quirk, R. P.; Monroy, V. M. *Ind. J. Technol.* **1993**, 31, 204–221.

(52) Mansson, P. *J. Polym. Sci., Polym. Chem. Ed.* **1980**, 18, 1945–1956.

(49) Arbusov, B. A. *Pure Appl. Chem.* **1964**, 9, 307–335.

THF) PDI = 1.09, M_n = 1478. Termination of the polymerization with ethylene oxide gas affords higher yields. Flash chromatography on ethylene oxide terminated polymerizations used 50% CH₂Cl₂/hexanes followed by CH₂Cl₂ to afforded pure material.

4-tert-Butyldimethylsilyloxybenzaldehyde (1). *tert*-Butyldimethylsilyl chloride (19.43 g, 129 mmol, 1.05 equiv) and imidazole (8.78 g, 129 mmol, 1.05 equiv) were dissolved in 300 mL of CH₂Cl₂ under N₂. 4-Hydroxybenzaldehyde (14.9 g, 123 mmol, 1.0 equiv) was added, and the solution stirred overnight. The solution was diluted with H₂O and washed twice with 1 N HCl, followed by saturated aqueous NaHCO₃. The organic layer was collected, dried, filtered, and condensed by rotatory evaporation. Filtration through a plug of silica gel in 50% CH₂Cl₂/hexanes afforded **1** quantitatively as a slightly golden oil (29.1 g, 100% yield). R_f = 0.5 (50% CH₂Cl₂/hexanes); ¹H NMR (300 MHz, CDCl₃) δ 9.88 (s, 1H), 7.79 (d, J = 8.4 Hz, 2H), 6.93 (d, J = 8.9 Hz, 2H), 0.99 (s, 9H), 0.25 (s, 6H); ¹³C NMR (125 MHz, CDCl₃, APT) δ 190.8, 161.5, 131.9, 120.5, 25.5, 19.1, -4.4; EI-MS m/z 236 (M⁺), 179 (M-*tert*-butyl).

Diethyl-4-cyanobenzylphosphonate (2). From the Arbuzov conditions **2** was obtained as a clear, colorless oil after column chromatography (4.5 g, 65% yield). R_f = 0.27 (40% EtOAc/CH₂Cl₂); ¹H NMR (300 MHz, CDCl₃) δ 7.62 (d, J = 7.6 Hz, 2H), 7.42 (dd, J = 8.0, 2.3 Hz, 2H), 4.05 (m, 4H), 3.20 (d, J = 22.0 Hz, 2H), 1.26 (t, J = 6.9 Hz, 6H).

4-(2-(4-tert-Butyldimethylsilyloxyphenyl)-(E)-1-ethenyl)-1-benzonitrile (3). Compound **3** was prepared via Horner-Emmons chemistry with compounds **1** and **2** in 90% yield (3.3 g). R_f = 0.21 (30% CH₂Cl₂/hexanes); ¹H NMR (300 MHz, CDCl₃) δ 7.62 (d, J = 8.5 Hz, 2H), 7.54 (d, J = 8.4 Hz, 2H), 7.42 (d, J = 8.4 Hz, 2H), 7.17 (d, J = 16.2 Hz, 1H), 6.95 (d, J = 16.0 Hz, 1H), 6.86 (d, J = 8.7 Hz, 2H), 0.99 (s, 9H), 0.21 (s, 6H); ¹³C NMR (125 MHz, CDCl₃, APT) δ 156.5, 142.4, 132.6, 132.2, 129.8, 128.4, 126.7, 124.8, 120.6, 119.3, 110.2, 25.8, -4.4; EI-MS m/z 335 (M⁺), 278 (M-*tert*-butyl); Anal. Calcd C₂₁H₂₅NOSi (335.523): C, 75.18; H, 7.51; N, 4.17; Si, 8.37. Found: C, 75.16; H, 7.62; N, 3.89; Si, 8.63.

4-(2-(4-tert-Butyldimethylsilyloxyphenyl)-(E)-1-ethenyl)-1-benzaldehyde (4). Stilbene **3** (1.36 g, 4.0 mmol, 1.0 equiv) was dissolved in 60 mL of Et₂O and cooled to -78 °C. DIBALH (7.31 mL, 7.3 mmol, 1.8 equiv, 1.0 M in hexane) was added to the solution dropwise via syringe in two equal portions. The reaction was stirred for 7 h at -78 °C and then for 30 min at 0 °C. The reaction was transferred via cannula onto vigorously stirring 10% AcOH/H₂O (250 mL) and stirred until the ether layer separated from the aqueous layer. The ether layer was washed twice with saturated aqueous NaHCO₃, collected, dried, filtered, and condensed by rotatory evaporation. Flash chromatography on silica gel using 30% CH₂Cl₂/hexanes yielded a pale yellow solid (1.24 g, 90% yield). R_f = 0.33 (40% CH₂Cl₂/hexanes); ¹H NMR (300 MHz, CDCl₃) δ 9.98 (s, 1H), 7.86 (d, J = 8.3 Hz, 2H), 7.62 (d, J = 8.3 Hz, 2H), 7.43 (d, J = 8.7 Hz, 2H), 7.21 (d, J = 16.2 Hz, 1H), 7.00 (d, J = 16.4 Hz, 1H), 6.86 (d, J = 8.7 Hz, 2H), 0.99 (s, 9H), 0.22 (s, 6H); ¹³C NMR (125 MHz, THF) δ 191.5, 157.2, 144.8, 136.6, 132.6, 131.6, 130.8, 129.2, 127.6, 126.4, 121.3, 26.3, 19.1, -4.14; EI-MS m/z 338 (M⁺), 281 (M-*tert*-butyl). HRMS (EI) C₂₁H₂₆O₂Si calcd 338.1702; found 338.1702.

4-(2-(4-(2-(4-tert-Butyldimethylsilyloxyphenyl)-(E)-1-ethenyl)-phenyl)-(E)-1-ethenyl)-1-benzonitrile (5). Horner-Emmons conditions yielded **5** as a yellow crystalline solid (2.24 g, 91% yield). R_f = 0.2 (30% CH₂Cl₂/hexanes); ¹H NMR (300 MHz, CDCl₃) δ 7.64 (d, J = 8.0 Hz, 2H), 7.58 (d, J = 8.3 Hz, 2H), 7.51 (m, 4H), 7.41 (d, J = 7.9 Hz, 2H), 7.21 (d, J = 16.7 Hz, 1H), 7.10 (d, J = 15.6 Hz, 1H), 7.09 (d, J = 16.3 Hz, 1H), 6.97 (d, J = 16.4 Hz, 1H), 6.84 (d, J = 7.6 Hz, 2H), 1.00 (s, 9H), 0.22 (s, 6H); ¹³C NMR (125 MHz, CDCl₃, APT) δ 156.3, 142.5, 138.6, 135.9, 133.1, 132.4, 131.1, 129.3, 128.3, 127.8, 127.2, 126.5, 121.0, 119.6, 111.0, 26.0; HRMS (EI) C₂₉H₃₁NOSi calcd 437.2175; found 437.2179; Anal. Calcd C₂₉H₃₁NOSi (437.659): C, 79.59; H, 7.14; N, 3.20; Si, 6.42. Found: C, 79.62; H, 6.92; N, 3.28; Si, 6.70.

Diethyl Benzylphosphonate (6). Arbuzov conditions afforded a clear, colorless oil after column chromatography (2.0 g, 76% yield). R_f = 0.28 (20% EtOAc/CH₂Cl₂); ¹H NMR (500 MHz, CDCl₃) δ 7.27 (m,

5H), 4.00 (m, 4H), 3.15 (d, J = 21.5 Hz, 2H), 1.24 (t, J = 7.3 Hz, 6H) plus (EtO)₂POH as an impurity; EI-MS m/z 229 (M⁺).

1-(4-tert-Butyldimethylsilyloxyphenyl)-2-(4-(2-phenyl-(E)-1-ethenyl)phenyl)-(E)-1-ethene (7). Compound **7** was obtained as white crystals using Horner-Emmons chemistry (0.520 g, 91% yield). ¹H NMR (500 MHz, THF-*d*₈) δ 7.54 (d, J = 7.1 Hz, 2H), 7.52 (m, 2H), 7.50 (d, J = 8.6 Hz, 2H), 7.43 (d, J = 8.6 Hz, 2H), 7.32 (t, J = 7.7 Hz, 2H), 7.21 (d, J = 7.5 Hz, 1H), 7.18 (s, 2H), 7.14 (d, J = 16.5 Hz, 1H), 7.04 (d, J = 16.5 Hz, 1H), 6.84 (d, J = 8.6 Hz, 2H), 0.99 (s, 9H), 0.22 (s, 6H); ¹³C NMR (125 MHz, THF-*d*₈, APT) δ 156.6, 138.8, 138.4, 137.6, 132.3, 129.6, 129.3, 129.3, 129.2, 128.7, 128.4, 127.8, 127.6, 127.5, 127.4, 121.2, 26.3, -4.2; EI-MS m/z 412 (M⁺), 355 (M-*tert*-butyl); HRMS (EI) C₂₈H₃₂O₂Si calcd 412.2222; found 412.2229.

4-(2-(4-(2-(4-Hydroxyphenyl)-(E)-1-ethenyl)phenyl)-(E)-1-ethenyl)-1-benzonitrile (8). Compound **5** (0.400 g, 0.91 mmol, 1.0 equiv) was taken up in 13 mL of THF. TBAF (0.91 mL, 0.91 mmol, 1 equiv, 1.0M in THF) was added dropwise via syringe. After 5 min, several drops of 10% AcOH/THF were added. The solvent was removed and the remaining orange solid washed with hexanes and then H₂O. After drying under vacuum overnight, an orange solid was obtained (0.228 g, 99% yield). R_f = 0.24 (CH₂Cl₂); ¹H NMR (300 MHz, THF-*d*₈) δ 7.70 (d, J = 8.8 Hz, 2H), 7.67 (d, J = 8.0 Hz, 2H), 7.55 (d, J = 8.5 Hz, 2H), 7.51 (d, J = 8.3 Hz, 2H), 7.38 (d, J = 8.6 Hz, 2H), 7.35 (d, J = 16.8 Hz, 1H), 7.23 (d, J = 16.3 Hz, 1H), 7.14 (d, J = 16.5 Hz, 1H), 6.97 (d, J = 16.5 Hz, 1H), 6.74 (d, J = 8.9 Hz, 2H); ¹³C NMR (125 MHz, THF-*d*₈, APT) δ 159.1, 143.3, 139.7, 136.5, 133.4, 133.1, 130.3, 129.9, 128.8, 128.3, 128.0, 127.5, 127.2, 125.8, 119.5, 116.5, 111.8; EI-MS m/z 323 (M⁺); HRMS C₂₃H₁₇NO calcd 323.1310; found 323.1306.

4-(2-(4-(2-phenyl-(E)-1-ethenyl)phenyl)-(E)-1-ethenyl)-1-phenol (9). TBAF (0.53 mL, 0.53 mmol, 1.1 equiv, 1.0 M in THF) was added slowly to **7** (0.200 g, 0.48 mmol, 1.0 equiv) in 12 mL of THF. After stirring for 5 min, several drops of 10% AcOH/THF were added. The solvent was evaporated in vacuo, and the crude product was purified by flash chromatography on silica gel using CH₂Cl₂ as eluant to give a tan solid (0.094 g, 65% yield). R_f = 0.28 (CH₂Cl₂); ¹H NMR (500 MHz, THF-*d*₈) δ 7.53 (d, J = 8.2 Hz, 2H), 7.51 (d, J = 8.6 Hz, 2H), 7.49 (d, J = 8.4 Hz, 2H), 7.37 (d, J = 8.4 Hz, 2H), 7.31 (t, J = 7.6 Hz, 2H), 7.20 (d, J = 7.4 Hz, 1H), 7.17 (s, 2H), 7.11 (d, J = 16.4 Hz, 1H), 6.97 (d, J = 16.4 Hz, 1H), 6.73 (d, J = 8.6 Hz, 2H); ¹³C NMR (125 MHz, THF-*d*₈, APT) δ 158.9, 138.9, 138.7, 137.4, 132.1, 129.6, 129.6, 129.4, 129.1, 128.8, 128.4, 127.8, 127.5, 127.4, 126.1; EI-MS m/z 298 (M⁺).

4-(2-(4-(2-(4-tert-Butyldimethylsilyloxyphenyl)-(E)-1-ethenyl)-phenyl)-(E)-1-ethenyl)-1-benzaldehyde (10). A turbid yellow solution of **5** (10.00 g, 22.8 mmol, 1.0 equiv) in 1000 mL of THF was cooled to -78 °C then DIBALH (22.8 mL, 22.8 mmol, 1 equiv, 1.0 M in hexane) was added. The reaction was warmed to 0 °C and stirred overnight. Another 1 equiv of DIBALH was added and the reaction warmed to room temperature. The reaction was cannulated onto 1000 mL of stirring 10% AcOH/H₂O. CH₂Cl₂ was added, and then the reaction mixture washed twice with saturated aqueous NaHCO₃, after which the organic layer was dried, filtered, and evaporated in vacuo. The crude product was purified by flash chromatography using CH₂Cl₂ to afford a yellow powder (8.41 g, 83% yield). R_f = 0.16 (40% CH₂Cl₂/hexanes); ¹H NMR (500 MHz, THF-*d*₈) δ 9.95 (s, 1H), 7.86 (d, J = 8.1 Hz, 2H), 7.74 (d, J = 8.1 Hz, 2H), 7.58 (d, J = 8.3 Hz, 2H), 7.54 (d, J = 8.3 Hz, 2H), 7.45 (d, J = 8.6 Hz, 2H), 7.38 (d, J = 16.4 Hz, 1H), 7.28 (d, J = 16.4 Hz, 1H), 7.17 (d, J = 16.4 Hz, 1H), 7.05 (d, J = 16.3 Hz, 1H), 6.84 (d, J = 8.4 Hz, 2H), 0.99 (s, 9H), 0.22 (s, 6H); ¹³C NMR (125 MHz, THF) δ 183.2, 156.6, 144.5, 139.2, 136.9, 132.6, 132.1, 130.8, 129.6, 128.8, 128.7, 128.2, 127.9, 127.8, 127.6, 127.2, 121.2, 26.2, 19.0, -4.1; EI-MS m/z 440 (M⁺); HRMS (EI) C₂₉H₃₂O₂Si calcd 440.2171; found 440.2168.

4-(2-(4-(2-(4-Hydroxyphenyl)-(E)-1-ethenyl)phenyl)-(E)-1-ethenyl)-1-benzaldehyde (11). To a solution of **10** (1.454 g, 3.3 mmol, 1.0 equiv) in 500 mL of THF was added TBAF (3.3 mL, 3.3 mmol, 1 equiv, 1.0 M in THF), and the solution was stirred for 5 min. The reaction was then quenched with several drops of 10% AcOH/THF. The solvent was removed in vacuo to afford an orange solid. This solid was taken up in 25 mL of CH₂Cl₂ and precipitated with 25 mL of hexanes. The

orange solid was collected by filtration and dried overnight to afford **11** (1.001 g, 76% yield). $^1\text{H NMR}$ (500 MHz, THF- d_8) δ 9.95 (s, 1H), 7.86 (d, $J = 8.2$ Hz, 2H), 7.73 (d, $J = 8.2$ Hz, 2H), 7.57 (d, $J = 8.2$ Hz, 2H), 7.51 (d, $J = 8.4$ Hz, 2H), 7.38 (d, $J = 8.6$ Hz, 2H), 7.38 (d, $J = 16.3$ Hz, 1H), 7.27 (d, $J = 16.5$ Hz, 1H), 7.14 (d, $J = 16.3$ Hz, 1H), 6.98 (d, $J = 16.3$ Hz, 1H), 6.74 (d, $J = 8.6$ Hz, 2H); EI-MS m/z 326 (M^+); HRMS (EI) $\text{C}_{23}\text{H}_{18}\text{O}_2$ calcd 326.1306; found 326.1298.

4-(2-(4-(2-(4-*tert*-Butyldimethylsilyloxyphenyl)-(E)-1-ethenyl)-phenyl)-(E)-1-ethenyl)-1-benzyl alcohol (12). Compound **10** (5.14 g, 11.6 mmol, 1.0 equiv) was dissolved in 500 mL of THF and cooled to -78 °C. DIBALH (23.2 mL, 23.2 mmol, 2 equiv, 1.0 M in THF) was added slowly, and then the reaction was warmed to room temperature and stirred 2 h. The reaction was cannulated onto stirring 10% AcOH/ H_2O , and after several minutes CH_2Cl_2 was added. The CH_2Cl_2 layer was then washed twice with saturated aqueous NaHCO_3 , after which it was dried, filtered, and evaporated in vacuo. The crude product was purified by flash chromatography on silica gel using CH_2Cl_2 as eluant to give a pale yellow powder (4.33 g, 84% yield). $R_f = 0.23$ (CH_2Cl_2); $^1\text{H NMR}$ (500 MHz, CDCl_3) δ 7.52 (d, $J = 8.1$ Hz, 2H), 7.49 (m, 4H), 7.40 (d, $J = 8.6$ Hz, 2H), 7.37 (d, $J = 8.1$ Hz, 2H), 7.11 (s, 2H), 7.08 (d, $J = 16.3$ Hz, 1H), 6.98 (d, $J = 16.3$ Hz, 1H), 6.84 (d, $J = 8.5$ Hz, 2H), 4.71 (s, 2H), 0.99 (s, 9H), 0.22 (s, 6H); $^{13}\text{C NMR}$ (125 MHz, CDCl_3 , APT) δ 156.6, 143.6, 138.3, 137.8, 137.3, 132.3, 129.2, 129.1, 128.7, 127.7, 127.4, 127.3, 121.2, 64.8, 26.3, -4.2 ; EI-MS m/z 442 (M^+), 385 (*M-tert-butyl*); HRMS (EI) $\text{C}_{29}\text{H}_{34}\text{O}_2\text{Si}$ calcd 442.2328; found 442.2333.

1-(2-(4-(2-(4-Bromomethylphenyl)-(E)-1-ethenyl)phenyl)-(E)-1-ethenyl)-4-*tert*-butyldimethylsilyloxybenzene (13). Compound **12** (0.200 g, 0.45 mmol, 1.0 equiv) was dissolved in 20 mL of THF, followed by the portionwise addition of NBS (0.104 g, 0.59 mmol, 1.3 equiv), and PPh_3 (0.154 g, 0.59 mmol, 1.3 equiv) to the stirring solution. The reaction was stirred for 6 h, diluted with CH_2Cl_2 , and then washed with H_2O , 1 N HCl, and saturated aqueous NaCl. The organic layer was collected, dried, filtered, and evaporated in vacuo to give a crude tan solid. This solid was dissolved in a minimum of CH_2Cl_2 and precipitated with hexanes. The crystals were collected, washed with 5% CH_2Cl_2 /hexanes, and dried to afford yellow plates of **13** (0.182 g, 80% yield). $R_f = 0.38$ (30% CH_2Cl_2 /hexanes); $^1\text{H NMR}$ (500 MHz, CDCl_3) δ 7.49 (m, 6H), 7.40 (d, $J = 8.4$ Hz, 2H), 7.38 (d, $J = 8.1$ Hz, 2H), 7.11 (d, $J = 16.3$ Hz, 1H), 7.10 (d, $J = 16.3$ Hz, 1H), 7.07 (d, $J = 16.3$ Hz, 1H), 6.97 (d, $J = 16.3$ Hz, 1H), 6.84 (d, $J = 8.6$ Hz, 2H), 4.52 (s, 2H), 0.99 (s, 9H), 0.22 (s, 6H); $^{13}\text{C NMR}$ (125 MHz, THF- d_8 , APT) δ 156.6, 138.9, 138.6, 138.6, 137.5, 132.3, 130.6, 130.0, 129.3, 128.7, 128.5, 127.9, 127.7, 127.4, 121.2, 34.3, 26.3, -4.2 ; EI-MS m/z 506 (M^+ , ^{81}Br), 504 (M^+ , ^{79}Br), 449 (*M-tert-butyl*, ^{81}Br), 447 (*M-tert-butyl*, ^{79}Br); HRMS (EI) $\text{C}_{29}\text{H}_{33}\text{OBrSi}$ calcd 504.1484; found 504.1486.

Diethyl 4-(2-(4-(2-(4-*tert*-butyldimethylsilyloxyphenyl)-(E)-1-ethenyl)phenyl)-(E)-1-ethenyl)-1-benzylphosphonate (14). Compound **13** was treated with general Arbuzov conditions to afford **14** as a yellow solid (0.160 g, 87% yield). $^1\text{H NMR}$ (500 MHz, CDCl_3) δ 7.48 (s, 4H), 7.47 (d, $J = 8.4$ Hz, 2H), 7.42 (d, $J = 8.6$ Hz, 2H), 7.30 (d, $J = 8.1$ Hz, 2H), 7.09 (s, 2H), 7.07 (d, $J = 16.3$ Hz, 1H), 6.97 (d, $J = 16.3$ Hz, 1H), 6.84 (d, $J = 8.4$ Hz, 2H), 4.03 (m, 4H), 3.16 (d, $J = 21.8$ Hz, 2H), 1.26 (t, $J = 7.0$ Hz, 6H), 0.99 (s, 9H), 0.22 (s, 6H); FAB-MS m/z 563 (M^+).

Dimethylhexylsilyl-4-(hydroxyphenyl)benzoate (15). A solution of morpholine (0.9 mL, 10.3 mmol, 1.1 equiv), 4'-hydroxy-4-biphenylcarboxylic acid (2.0 g, 9.3 mmol, 1.0 equiv), and dimethylformamide (10 mL) was stirred as dimethylhexylsilyl chloride (1.8 mL, 11.1 mmol, 1.2 equiv) was added. The solution was stirred for an additional 30 min at room temperature. The resulting mixture was diluted with CH_2Cl_2 , washed with saturated aqueous NaHCO_3 and water, and then dried. The solvent was removed by rotary evaporation, and the product was purified by flash chromatography on silica gel using CH_2Cl_2 to give **15** as a tacky, white solid (2.8 g, 86% yield). $^1\text{H NMR}$ (500 MHz, CDCl_3) δ 8.07 (d, $J = 8.1$ Hz, 2H), 7.61 (d, $J = 8.2$ Hz, 2H), 7.53 (d, $J = 8.4$ Hz, 2H), 6.93 (d, $J = 8.4$ Hz, 2H), 1.75 (septet, $J = 6.8$ Hz, 1H), 1.00 (s, 6H), 0.96 (d, $J = 6.8$, 6H), 0.44 (s, 6H); $^{13}\text{C NMR}$ (125 MHz, CDCl_3 , APT) δ 167.9, 157.2, 146.2, 132.9, 131.4, 130.2, 129.3, 127.2, 116.7, 34.8, 20.8, 19.2, -2.0 .

4-(4-Oligo(9)styrene-*b*-oligo(9)isoprenecarbonyloxyphenyl) Benzoic Acid (16). General esterification procedure followed by general deprotection conditions afforded **16** as a white solid (1.2 g, 75% yield). $^1\text{H NMR}$ (400 MHz, CDCl_3) δ 8.31 (d, $J = 8.2$ Hz, 2H), 7.62 (d, $J = 8.4$ Hz, 2H), 7.38 (d, $J = 8.4$ Hz, 2H), 7.31 (d, $J = 8.2$ Hz, 2H), 7.00 (br m, 46H), 4.64 (br m, 11H), 3.30 (br m, 2H), 1.40 (br m, 100H); GPC (254 nm, THF) PDI=1.08, $M_n=1740$.

4-(4-(4-(4-Oligo(9)styrene-*b*-oligo(9)isoprenecarbonyloxy)phenyl)benzoyloxy)phenyl)benzoic Acid (17). General esterification procedure followed by general deprotection conditions afforded **17** as a white solid (0.80 g, 78% yield). $^1\text{H NMR}$ (400 MHz, CDCl_3) δ 8.35 (d, $J = 8.2$ Hz, 2H), 7.79 (d, $J = 8.4$ Hz, 2H), 7.62 (m, 4H), 7.37 (d, $J = 8.4$ Hz, 2H), 7.32 (d, $J = 8.2$ Hz, 2H), 7.00 (br m, 50H), 4.66 (br m, 12H), 3.30 (br m, 2H), 1.40 (br m, 100H); GPC (254 nm, THF) PDI = 1.08, $M_n = 1900$.

4-(2-(4-(2-(4-(4-(4-Oligo(9)styrene-*b*-oligo(9)isoprenecarbonyloxy)phenyl)benzoyloxy)phenyl)benzoyloxy)phenyl)-(E)-1-ethenyl)-phenyl)-(E)-1-ethenyl) Benzonitrile (18). General esterification procedure afforded **18** as a yellow solid (0.104 g, 91% yield). $^1\text{H NMR}$ (400 MHz, CD_2Cl_2) δ 8.31 (d, $J = 8.4$ Hz, 4H), 7.76 (m, 6H), 7.68 (m, 8H), 7.59 (m, 3H), 7.41 (d, $J = 8.4$ Hz, 2H), 7.00 (br m, 50H), 4.66 (br m, 11H), 3.30 (br m, 2H), 1.40 (br m, 100H); GPC (254 nm, THF) PDI=1.12, $M_n=2240$.

4-(2-(4-(2-(4-(4-(4-Oligo(11)styrene-*b*-oligo(15)isoprenecarbonyloxy)phenyl)benzoyloxy)phenyl)benzoyloxy)phenyl)-(E)-1-ethenyl)phenyl)-(E)-1-ethenyl) Benzonitrile (19). General esterification procedure afforded **19** as a yellow solid (0.250 g, 89% yield). $^1\text{H NMR}$ (400 MHz, CD_2Cl_2) δ 8.31 (d, $J = 8.4$ Hz, 4H), 7.76 (m, 6H), 7.68 (m, 8H), 7.59 (m, 3H), 7.41 (d, $J = 8.4$ Hz, 2H), 7.00 (br m, 57H), 4.66 (br m, 22H), 3.30 (br m, 2H), 1.40 (br m, 140H); GPC (254 nm, THF) PDI=1.12, $M_n = 2758$.

4-(2-(4-(2-(4-(4-(4-Oligo(13)styrene-*b*-oligo(16)isoprenecarbonyloxy)phenyl)benzoyloxy)phenyl)benzoyloxy)phenyl)-(E)-1-ethenyl)phenyl)-(E)-1-ethenyl) Benzonitrile (20). General esterification procedure afforded **20** as a yellow solid (0.203 g, 85% yield). $^1\text{H NMR}$ (400 MHz, CD_2Cl_2) δ 8.31 (d, $J = 8.4$ Hz, 4H), 7.76 (m, 6H), 7.68 (m, 8H), 7.59 (m, 3H), 7.41 (d, $J = 8.4$ Hz, 2H), 7.00 (br m, 72H), 4.66 (br m, 24H), 3.30 (br m, 2H), 1.40 (br m, 150H); GPC (254 nm, THF) PDI = 1.08, $M_n = 3268$.

4-(2-(4-(2-(4-(4-(4-Oligo(9)styrene-*b*-oligo(9)isoprenecarbonyloxy)phenyl)benzoyloxy)phenyl)benzoyloxy)phenyl)-(E)-1-ethenyl)-phenyl)-(E)-1-ethenyl)benzene (21). Rodcoil **21** was obtained from general esterification procedure as a white solid (0.091 g, 70% yield). $^1\text{H NMR}$ (400 MHz, CD_2Cl_2) δ 8.29 (d, $J = 8.6$ Hz, 4H), 7.79 (m, 6H), 7.71 (m, 2H), 7.63 (d, $J = 8.6$ Hz, 2H), 7.56 (s, 4H), 7.55 (d, $J = 7.6$ Hz, 2H), 7.39 (m, 4H), 7.00 (br m, 48H), 4.66 (br m, 15H), 3.30 (br m, 2H), 1.40 (br m, 100H); GPC (254 nm, THF) PDI = 1.12, $M_n = 2317$.

4-(2-(4-(2-(4-Oligo(9)styrene-*b*-oligo(9)isoprenecarbonyloxy)phenyl)-(E)-1-ethenyl)phenyl)-(E)-1-ethenyl) Benzonitrile (22). General esterification procedure afforded **18** as a yellow solid (0.079 g, 97% yield). $^1\text{H NMR}$ (400 MHz, CD_2Cl_2) δ 7.67 (d, $J = 8.4$ Hz, 2H), 7.64 (d, $J = 8.4$ Hz, 2H), 7.57 (m, 6H), 7.27 (d, $J = 16.29$ Hz, 1H), 7.00 (br m, 47H), 4.66 (br m, 14H), 3.30 (br m, 2H), 1.40 (br m, 100H); GPC (254 nm, THF) PDI = 1.11, $M_n = 1716$.

4-(2-(4-(2-(4-Oligo(9)styrene-*b*-oligo(9)isoprenecarbonyloxy)phenyl)-(E)-1-ethenyl)phenyl)-(E)-1-ethenyl)benzaldehyde (23). General esterification procedure afforded **23** as a yellow solid (0.235 g, 66% yield). $^1\text{H NMR}$ (400 MHz, CD_2Cl_2) δ 9.95 (s, 1H), 7.87 (d, $J = 8.3$ Hz, 2H), 7.70 (d, $J = 8.1$ Hz, 2H), 7.57 (m, 6H), 7.30 (d, $J = 16.6$ Hz, 1H), 7.00 (br m, 54H), 4.64 (br m, 20H), 3.26 (br m, 2H), 1.40 (br m, 100H); GPC (254 nm, THF) PDI = 1.11, $M_n = 1793$.

4-(Oligo(9)styrene-*b*-oligo(9)isoprenecarbonyloxy-*b*-(5)phenylene vinylene)phenol (24). General Horner-Emmons followed by deprotection conditions afforded **24** as a yellow solid after several silica gel purifications (0.032 g, 35% yield for 2 steps). $^1\text{H NMR}$ (500 MHz, CD_2Cl_2) δ 7.00 (br m, 54H), 4.64 (br m, 20H), 3.26 (br m, 2H), 1.40 (br m, 100H); GPC (254 nm, THF) PDI = 1.08, $M_n = 2857$.

4-(2-(4-(2-(4-Oligo(11)styrene-*b*-oligo(16)isopreneethyloxy)phenyl)-(E)-1-ethenyl)phenyl)-(E)-1-ethenyl)benzaldehyde (25). The mesylated coil (0.250 g, 0.1 mmol, 1.0 equiv.), **11** (0.037 g, 0.11 mmol, 1.1

equiv.), Cs₂CO₃ (0.105 g, 0.3 mmol, 3.0 equiv.), and tetrabutylammonium bromide (0.006 g, 0.02 mmol, 0.2 equiv.) were taken up in 90 mL of THF. A distillation head was attached and the suspension heated in an oil bath to 70 °C for 48 h. The oil bath was removed and the solvent removed in vacuo to give a crude orange paste. This material was purified by dissolving in CH₂Cl₂ and precipitating into MeOH followed by flash chromatography on silica gel using CH₂Cl₂ as eluant giving **25** as an orange solid after evaporation (0.235 g, 86% yield). ¹H NMR (500 MHz, CD₂Cl₂) δ 9.95 (s, 1H), 7.57 (m, 4H), 7.46 (m, 2H), 7.30 (d, *J* = 16.6 Hz, 1H), 7.00 (br m, 60H), 4.64 (br m, 26H), 3.26 (br m, 2H), 1.40 (br m, 145H).

4-(Oligo(11)styrene-*b*-oligo(16)isopreneethoxy-*b*-(5)phenylene vinylene)phenol (26). General Horner-Emmons followed by depro-

tection conditions afforded **26** as a yellow solid after several silica gel purifications (0.210 g, 50% yield for 2 steps). ¹H NMR (500 MHz, CD₂Cl₂) δ 7.00 (br m, 80H), 4.64 (br m, 24H), 3.26 (br m, 2H), 1.40 (br m, 145H).

Acknowledgment. Supported by grants from the Army Research Office (DAAH04-96-1-0450) and the Office of Naval Research (N00014-96-1-0515). G.N.T. thanks the Beckman Institute for Advanced Science and Technology at the University of Illinois for a 1997-98 research assistantship and the ACS Division of Organic Chemistry for a 1998-99 fellowship.

JA991506O